International Communications in Heat and Mass Transfer 153 (2024) 107370

Contents lists available at ScienceDirect

International Communications in Heat and Mass Transfer

journal homepage: www.elsevier.com/locate/ichmt

Evaluation and optimization of supercritical cycles using CO_2 based mixtures as working fluids: A thermodynamic study

Al Bara Shalaby [a], Nadeem Ahmed Sheikh [a,*], Abubakr Ayub [b], Muhammad Ahmed [c], Muhammad Imran [d], Muhammad Wakil Shahzad [e,*]

[a] Department of Mechanical Engineering, Faculty of Engineering & Technology, International Islamic University, Islamabad, Pakistan
[b] Net Zero Industry Innovation Center (NZIIC), Teesside University, Middlesbrough TS2 1DJ, United Kingdom
[c] Department of Mechanical Engineering, Capital University of Science and Technology (C.U.S.T), Islamabad, Pakistan
[d] Department of Mechanical, Biomedical and Design Engineering, Aston University, Birmingham B4 7ET, United Kingdom
[e] Department of Mechanical and Construction Engineering, Northumbria University, Newcastle upon Tyne NE1 8ST, United Kingdom

ARTICLE INFO

Keywords:
CO_2-based binary mixtures
Supercritical power cycles
Cycle specific work
Response surface method
Multi-objective optimization

ABSTRACT

This study focuses on the thermodynamic performance analysis and optimization of CO_2-based binary fluid mixtures in supercritical thermodynamic power cycles exploiting high-temperature waste heat. Response surface method is used to establish relationships between cycle performances and significant cycle parameters. Multi-objective optimization is carried out to obtain optimal solutions with higher cycle specific work and higher cycle efficiency. The analysis reveals that increasing additive molar fraction of the considered mixtures improves cycle thermodynamic performance. Among considered mixtures, the CO_2-R152a mixture exhibits a higher cycle specific work and a larger cycle efficiency. For instance, in the recompression cycle configuration, the CO_2-R152a mixture achieves cycle specific work of 83.9 kJ/kg and corresponding cycle efficiency of 37.2% at the optimal conditions. Comparative analysis demonstrates improved cycle-specific work for CO_2-based mixtures compared to supercritical pure CO_2 power cycles. In the recompression cycle configuration, the CO_2-R152a mixture shows an average increase of 12 kJ/kg in cycle specific work compared to the supercritical CO_2 power cycle. The simple recuperated cycle configuration exhibits an average increase of 13 kJ/kg. The utilization of these mixtures results in a substantial gain in cycle specific work, thereby contributing to enhanced energy efficiency and sustainability in high-temperature waste heat recovery applications.

1. Introduction

To tackle the issues of global warming and environmental constraints, significant changes are anticipated in global electricity production in the near future. Consequently, industries and researchers are experimenting with various strategies to meet these targets. In addition to proposing sustainable solutions, it is necessary to increase the energy efficiency of available facilities. Utilization of waste heat is one of the key factors in boosting energy efficiency. Waste heat recovery allows a reduction in the consumption of fossil fuels, in addition to related environmental impacts, carbon footprints, and greenhouse gas emissions [1]. This results in improved economic feasibility of the plant [2]. Several studies have evaluated the potential of waste heat in different industries at various locations, and the quality and quantity of waste heat that can be utilized from these sources.

In a study by Forman et al. [3], 72% of the primary energy consumption was estimated to be dissipated. Waste heat is often considered to be at low temperatures, which has low conversion efficiency according to the Carnot factor. Heat dissipation from the electricity sector is characterized by lower temperatures, while the industrial and transport sectors are often at higher temperatures, surpassing 100 °C. Despite this, the electricity sector dominates with nearly 107 PJ of dissipated heat, followed by the transportation and industrial sectors dissipating 62 PJ and 32 PJ, respectively. Galanis et al. [4] investigated the forms of energy released to the environment from industrial processes. They classified it into three main categories: exhaust at temperatures between 150 and 800 °C, vapors and gases with temperatures up to 500 °C, and steam at temperatures between 100 and 250 °C.

Papapetrou et al. [5] found that EU's industrial waste heat potential for temperatures above 500 °C amounts to 124 TWh/year, representing

* Corresponding authors.
E-mail addresses: a.sheikh@tees.ac.uk (N.A. Sheikh), muhammad.w.shahzad@northumbria.ac.uk (M.W. Shahzad).

https://doi.org/10.1016/j.icheatmasstransfer.2024.107370

Available online 8 March 2024

41% of the total. Another study [6] focused on waste heat at temperatures above 650 °C, dissipating from different industries in the US. They estimated the waste heat recovery potential to be equal to 113.6 TWh_{th}/year. However, heat recovery from these sources is challenging because of the presence of several reactive constituents in the exhaust streams. Firth et al. [7] estimated waste heat emissions globally from different sectors in 2030. Their study highlighted the need for WHR technologies that are effective at medium-to-high temperatures.

Waste heat as a possible energy source has many factors that affect it, making it difficult to recover heat, including user demand, available facilities, and characteristics of the waste heat source [8]. Currently, two main technologies to convert waste heat into electricity are steam cycle and organic Rankine cycle. Both work on the principle of Rankine cycle but they utilize different heat sources and applicable at different scales [9].

Superheated steam cycles are a common method used with applications of medium to large plant size (up to hundreds of MWs) at high temperatures from 400 °C to 700 °C. Steam Rankine cycles have lower conversion efficiencies when used in small applications or at temperatures up to 400 °C [10]. In contrast, the organic Rankine is used in low to medium temperatures of waste heat sources varying from 100 °C to 400 °C with output power ranging from a few kWs to tens of MWs. Owing to the organic working fluids adoption, the evaporation and condensation pressures were reduced and increased, respectively. The addition of organic fluids limits the cycle for temperatures up to 400 °C, owing to low thermal stability [11].

Another technology that reduces the gap between waste heat recovery applications and can compete with other cycles in terms of performance is the carbon dioxide power cycle. Feher [12] was the first to propose a closed supercritical carbon dioxide Brayton cycle. CO_2 power cycles, owing to the low critical point of carbon dioxide, are being studied under supercritical or trans-critical conditions. This provides an advantage for CO_2 to be used in waste heat applications with a wide range of temperatures as compared to steam cycles that run at high temperatures or organic Rankine cycles, which are used at low temperatures [13]. CO_2 has various advantages when used as the working fluid. It is non-toxic, non-combustible, can reach high temperatures (higher than 500 °C [14]), and is abundant in nature. Also due to the physical properties of CO_2, the losses associated with heat transfer between the source and working fluid are reduced. In addition to their compact turbomachinery, and high flexibility [15].

sCO_2 cycles have been studied for use with nuclear energy [16], concentrating solar power [17] or as bottoming cycles for gas turbines [18]. Due to its favorable properties, studies were conducted to replace the organic Rankine cycle for medium-temperature applications [19]. Due to the variety of applicable use cases and temperatures, the cycle configurations vary accordingly. Cycles can be simple layouts containing a minimum number of components, such as a simple recuperated layout, or more complex layouts with more components. In addition, there are patented cycles owned by specialized companies like ECHOGEN [20].

To compare recompression and single recuperated cycles for a temperature range of up to 830 °C for waste heat recovery applications and achieving a higher power output. The study showed that a single recuperated cycle performed best at temperatures below 450 °C [21]. Another study carried out by Martinez et al. [22] considered the same two cycles in addition to the precompression cycle for a source temperature of 600 °C from the exhaust of a gas turbine. The precompression cycle had the lowest performance, and the single recuperated cycle achieved the best performance in terms of power output.

Manente et al. [23] studied partial heating and Single flow split with dual expansion cycles for a gas turbine exhaust temperature of 600 °C. The partial heating cycle had a wider range of TIT, which achieved the highest performance, whereas the other cycle was limited to temperatures approaching 550 °C. Song et al. [24] compared the traditional Preheating cycle and preheating cycle with regeneration branch for WHR from a diesel engine exhaust at 300 °C. When a regeneration branch was added, greater performance was achieved. They concluded that heat transmission in the regenerator is restricted because of the high preheating temperature in the traditional design. Ahmed et al. [25] compared the performance of recompression and partial cooling cycles and studied the effect of varying ambient temperature and split ratio on their performance. The recompression cycle outperformed the other in terms of efficiency.

Despite the advantages of sCO_2 as a working fluid, its low critical point limits its application at low ambient temperatures. To alter the critical point of CO_2, researchers have introduced adding other fluids at different percentages to adapt their critical points based on their requirements [26]. Other objectives include increasing the expansion of the turbine and increasing the stability of the working fluid properties near the critical point [27]. The selection of the right additive can be challenging due to the need to satisfy multiple criteria set by researchers [28]. While finding the perfect additive is challenging and often requires compromise, accurate prediction of mixture properties in the absence of experimental data is essential. Some studies utilized available experimental (VLE) data to calibrate binary interaction parameters of property models [29].

Tafur et al. [30] evaluated the impact of the addition of additives to CO_2 and their effect on the efficiency of different cycle layouts. Based on their impacts on the critical temperature of the mixture, they categorized the additives into two categories. The first is additives that result in a decrease in the critical temperature, and the second is additives that result in an increase in the critical temperature. In [31], researchers aimed at reducing critical temperature to bring it closer to the low ambient temperature of 15 °C. They have selected Xe and Kr for the analysis. For the studied TIT of 550 °C, Kr was found to have huge thermo-economic potential as compared to pure CO_2.

Yang et al. [32] study concluded that the use of R32 as an additive improved thermal performance at 400 °C with relatively high ambient temperatures. A study by Ma et al. [33] involved a comparative analysis of various CO_2-based mixtures against pure CO_2 across a temperature range of 550 to 750 °C. Results indicated a notable enhancement in mixture performance as the working fluid, particularly at lower turbine inlet temperatures (TIT). Furthermore, under conditions of high TIT and elevated ambient temperatures, the integration of mixtures resulted in a reduction of exergy losses. In another study on additives, H_2S had the best thermodynamic performance while propane had the highest heat transfer coefficient in the recuperator [34].

Literature shows that CO_2 based mixtures offer greater potential especially when operating under various temperature ranges of both waste heat as well as ambient conditions. However, selecting the mixture is dependent on numerous factors and no comprehensive assessment is carried out in literature. Secondly, inter-dependencies of various cycle parameters in their ranges of operation(s) can lead to variabilities in the performances of different cycle configurations. The dependencies need more investigation and quantitative relationship(s). Thirdly, optimization of such cycle configurations is reported at a limited scale. Moreover, the recovery units of heat to power are primarily aimed to enhance power generation albeit at higher efficiencies and lower price-foot print. To address these gaps, this work presents a comprehensive framework encompassing mixture selection, accurate calculation of thermodynamic properties of mixture, parametric dependencies, and multi-objective optimization outcomes for selected mixtures, taking into account operational constraints.

The main contribution of this work is the thermodynamic optimization of cycle configurations with mixture working fluids subject to variation in working fluid mixture composition, cycle minimum temperature, cycle minimum pressure and split fraction. The change in cycle minimum temperature is studied to account for variation in ambient air temperature. The use of RSM allows to decide optimum operating conditions for different ambient temperature of plant site. Thus, the analysis

is generic and can be applicable to different plant sites located in different ambient temperature zones. Secondly, previous works on CO_2 mixtures primarily focused on cycle efficiency as a key performance indicator. However, in waste heat recovery, the important design variable to study should be cycle specific work in addition to cycle efficiency. Higher cycle specific work (kJ/kg) implies larger power output with a smaller working fluid inventory which is a cost-effective solution.

The overall paper is divided into the following steps. In the first stage, the additives for CO_2 mixtures are decided based on thermodynamic and environmental characteristics. In second stage, thermodynamic properties of the selected mixtures are computed. In the third stage, thermodynamic and performance study of two cycle layouts of supercritical cycles is performed adopting the selected CO_2-based mixtures as the working fluid. To decide optimum range of the molar composition of working fluid and the cycle parameters, the response surface methodology is used. Finally, multi-objective optimization is carried out to determine the optimal values for maximum performance by combining the two objective functions.

2. Selection and characterization of working fluids

2.1. Screening and selection of additive compounds for CO_2-based mixtures

The foremost requirement for designing a CO_2-based binary mixture as a working fluid for a supercritical power cycle is that the additive be thermally stable, at temperature greater than the cycle maximum temperature, that is, the turbine inlet temperature. The required thermal stability limit for the current scenario of waste heat recovery from high-temperature waste heat is 400–450 °C. The second major requirement is that the additive has a higher critical point temperature, which means that the value should be >31 °C to allow the cooler to operate at high environmental temperatures in a cycle.

The third main requirement is the additive's critical pressure, which need to be lower than the critical pressure of CO_2 to obtain a mixture with lower critical pressure and, in turn, lower operating pressures in the power cycle, which is advantageous considering component design.

Other characteristics included in the selection of additives are negligible ODP, low GWP, and nonflammability. The feature that is often overlooked during the selection of a suitable additive is the experimental fluid property information of the additive and the corresponding CO_2-based mixture. The availability of data enables the optimization of the property models specifically mixture binary interaction parameters.

The preliminary selection of additives and screening of suitable additives that meet the necessary criteria for various organic and inorganic compounds are carried out. The physical and environmental characteristics of the compounds used as additives are presented in Table 1. These include straight-chain hydrocarbons (propane), toxic substances (H_2S), aromatics (benzene and m-xylene), and natural and artificial refrigerants (R152a and R161). The main concept is to choose two additives that fit the criteria, belong to different classes of compounds, and study how they reflect on performance of the power cycle. Therefore, R152a and Benzene are selected because they meet all the criteria points defined for this study, except for one criterion, that is, the flammability of the compound. The high flammability of these compounds can be suppressed by mixing them with CO_2 in a CO_2-based binary mixture, where CO_2 is a fire-suppressant. Future research can expand the performance charts of supercritical cycles by considering additional CO_2 mixtures.

2.2. Thermodynamic properties of selected mixtures

The standard Peng-Robinson EoS built-in ASPEN Plus software is used to calculate the thermodynamic properties of pure fluids and the selected CO_2-based mixtures.

In literature [40,41], Standard Peng Robinson EoS is proven to be an accurate EoS to predict thermodynamic behavior of CO_2 based binary mixtures including vapor-liquid equilibrium (VLE) phase behavior, liquid densities, residual enthalpy and residual entropy. However, the predictive capability of EoS can be improved by optimizing binary interaction parameter ($k_{i,j}$) using the available experimental VLE data. Hence, the regression analysis is carried out for this purpose.

First, experimental VLE data available in ASPEN V11 NIST library for each of mixtures is used to prepare separate data sets. These datasets are then used for the regression analysis in ASPEN Plus. As a result, a new binary interaction parameter is calculated along with standard deviation.

Next, to verify the accuracy of the modified PR EoS, a comparison of predicted results using the modified PR EoS and different sets of experimental data is carried out. Table 2 presents the binary interaction parameters of CO_2/R152a and CO_2/C_6H_6 mixtures calculated using regression analysis, standard deviation is also reported.

For CO_2-R152a mixture, the experimental VLE data are retrieved from [42,43]. And for CO_2-C_6H_6 mixture, experimental VLE data are retrieved from [44,45]. Fig. 1 and Fig. 2 shows the predicted VLE data from modified PR EoS and experimental data; as evident, the predicted results from the modified PR EoS agreed well with the experimental data.

After verification of PR EoS, Pressure-Temperature envelopes are generated for each mixture at different compositions which are used to find vapor-liquid critical points. These critical points are plotted to represent the variation of critical properties of the mixture with the increase in the molar composition of the additive in the mixture.

Fig. 3 and Fig. 4 illustrate the critical point properties of the mixtures at different compositions. The critical point loci of R152a show an increase in the critical temperature with increase of additive composition, and a slight increase in the critical pressure then decrease at higher molar fraction of the additive as opposed to pure CO_2. The loci of C_6H_6 show an increase in critical temperature however, critical pressure

Table 2
Optimized binary interaction parameter (for the selected two mixtures).

Additive	Binary mixing parameter	Standard deviation
R152a	0.006436	0.002571
C_6H_6	0.076638	0.00486

Table 1
Thermophysical properties of shortlisted additives.

Sr	Additive	ODP [35–37]	GWP (100) [36–38]	T_{cr} [38] (°C)	P_{cr} [38] (bar)	Flammable [39]	Auto- ignition [35,36,38]	Boiling point [38] (°C)	Exp. Data [38]
1	H_2S	0	5.8	100.4	89.4	Yes	260	−60.3	✓
2	R161	0	12	102.2	50.9	Yes	N/A	−37.6	
3	Benzene	0	2.6	288.9	48.9	Yes	498	80.09	✓
4	M-xylene	0	10	344.8	34.5	Yes	527	139	
5	R152a	0	124	113.15	44.96	Yes	440	−24.7	✓
6	Propane	0	3	96.7	42.48	Yes	470	−42.1	✓

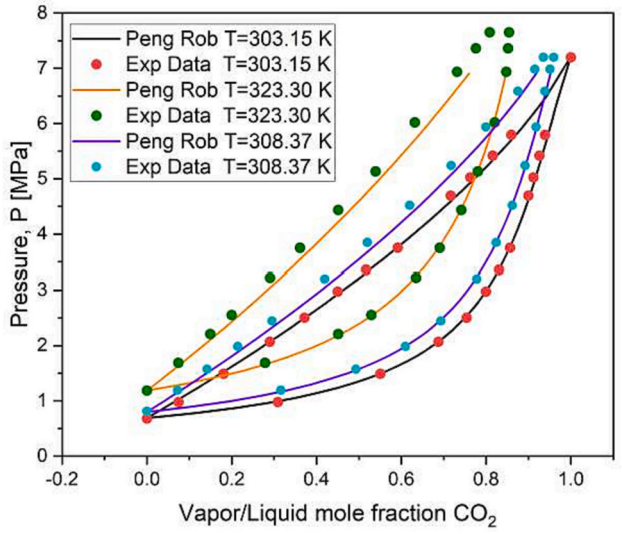

Fig. 1. Comparison of predicted and experimental VLE of CO_2/R152a mixture at different temperatures.

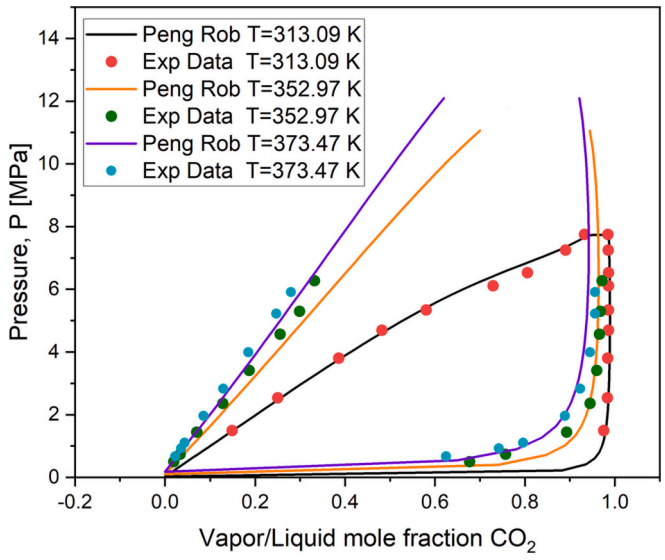

Fig. 2. Comparison of predicted and experimental VLE of CO_2/C_6H_6 mixture at different temperatures.

increases significantly and then reduces again to a lower point. As per the classifications of critical points developed by Konynenburg and Scott [46], both the selected mixtures belongs to Type-I with continuous vapor-liquid critical loci.

2.3. Selection of composition of CO_2-based mixtures

After calculating the vapor-liquid critical points using the optimized binary interaction parameter (k_{ij}), the decision of molar fractions to be considered for power cycle analysis is performed. Molar fractions of the mixtures need to ensure that cycles run at supercritical state at higher ambient temperatures ($T > 25$ °C). Table 3 shows the critical properties of the selected mixtures as working fluids in the supercritical power cycle.

Four compositions of each mixture are selected to achieve critical temperature close to 50 °C. while also maintaining the reasonable value of critical pressure. The higher critical temperature of the mixture enables the supercritical power cycle to achieve a higher cycle efficiency

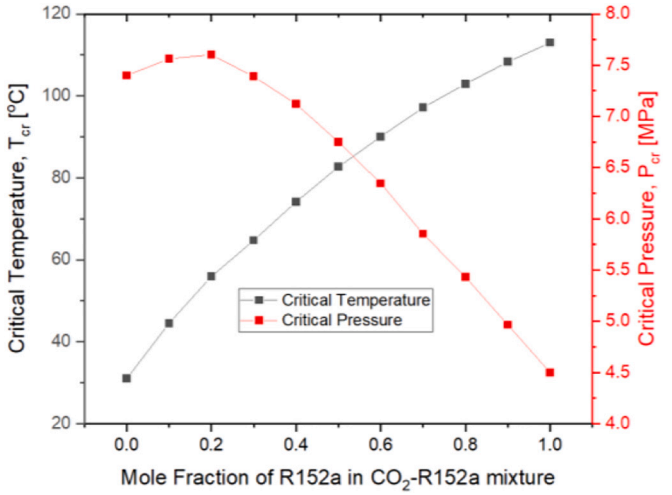

Fig. 3. Critical loci showing critical points at different compositions of CO_2/R152a mixture.

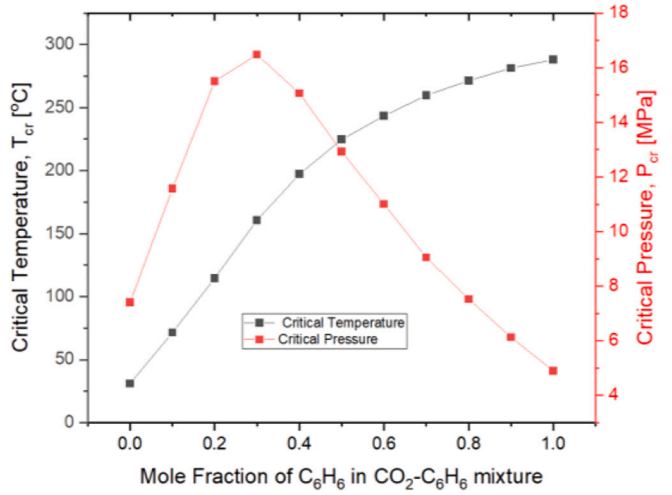

Fig. 4. Critical loci showing critical points at different compositions of CO_2/C_6H_6 mixture.

Table 3
Critical point properties of selected composition of CO_2-R152a and CO_2-C_6H_6 mixtures.

Percentage mole fraction of R152a	T_{cr} (°C)	P_{cr} (MPa)	Percentage mole fraction of C_6H_6	T_{cr} (°C)	P_{cr} (MPa)
0	31	7.38	0	31	7.38
5	37.6	7.52	1	36.2	7.81
10	44.5	7.56	2.3	42.5	8.39
15	50.1	7.63	3.6	48.6	8.99

under higher ambient temperature conditions, which cannot be achieved using pure CO_2 from a thermodynamic point of view.

3. Heat source and configurations of power cycles

The system consists mainly of a waste heat source and a power cycle. Both parts are connected by a heat exchanger. In this study, the waste heat source was considered to provide heat at a temperature of 500 °C. Table 4 lists the composition of the heat sources.

Numerous works [47,48] on selection of cycle layout of sCO_2 cycle for waste heat recovery are already carried out. Most of the works

Table 4
Composition of heat source gas components.

Sr	Component	% Vol
1	N_2	48.4
2	CO	17.3
3	H_2	13.3
4	CO_2	17
5	CH_4	4

recommend cascade cycle with single split, partial heating layout and dual split with dual expansion layout for high temperature waste heat recovery with the rationale to enhance power output and increase heat recovery of power cycle. In this study, simple recuperated and recompression cycle layouts are selected. The two layouts however do not comply with the layout selection of previous works on heat recovery because rationale is not to select suitable cycle layout instead the focus is to evaluate the thermodynamic implications of CO_2 based mixtures on thermodynamic performance of supercritical cycles.

In the simple recuperated cycle, a single recuperator is present that allows heat transfer from the flow leaving the turbine to the flow entering the main heater. Then the flow is cooled before the compression process resulting in reduced compressor workload. However, maintaining an equal mass flow in both sections of the recuperator may lead to a temperature imbalance at the hot end, potentially reducing overall efficiency. To avoid this, the recompression cycle is used where the flow leaving the cold side of the low-temperature recuperator is split into two flows, one leaving towards the cooler and then the compressor, and the second leaving the recompressor; both flows are then mixed after the hot end of the low-temperature recuperator. The concept of recompression CO_2 cycle layout is first given by [49].

4. Thermodynamic modeling

4.1. Governing equations

The thermodynamic model and governing equations used in this study are listed in Table 5. For thermodynamic performance evaluation, cycle specific work and cycle thermal efficiency are considered.

4.2. Simulation environment

The experiments are run on ASPEN Plus software with the modified PR EoS. Cycle layouts are designed as per Fig. 5 and Fig. 6. The input parameters and their corresponding values are listed in Table 6. The assumptions followed in this study state that cycles run at steady state flow conditions. The isentropic and mechanical efficiencies of turbomachinery are considered. Also, pressure losses for each component are included in the analysis.

Heat exchangers are modeled using 1 dimensional discretization method in which the heat exchanger is divided into 100 cells and temperature across each cell is calculated assuming constant thermal load of each cell. The overall model also ensures minimum internal temperature difference (MITA) to be equal to 15 $^{\circ}C$. To achieve the set MITA value at different input operating conditions, a design specification is set to vary the cold side outlet temperature of recuperator.

The mass flow rate of the heat source is optimized to achieve a fixed turbine inlet temperature. Cycle minimum temperature, turbine expansion pressure and mass split ratio are varied in a specified range while cycle maximum pressure and mass flow rate are constants. The input parameters used in the simulations are listed in Table 6. Turbomachinery efficiencies are considered from [50].

Pressure losses in heat exchanger units are considered [51]. Their percentages are 1% in the main heater and 0.5% in the cooler. In the recuperator, the pressure losses are 1.5% and 0.5% at the low and high-pressure sides, respectively.

Table 5
Governing equations used in this study.

Parameter	Unit	Equation	
$T_{\min}$	$^{\circ}$C	$T_{amb} + 15^{\circ}$C	(1)
P_{loss}	–	$(P_{in} - P_{out})/P_{in}$	(2)
$W_{\text{compression}}$	kJ/kg	$h_{compressor\ outlet} - h_{compressor\ inlet}$	(3)
$W_{\text{expansion}}$	kJ/kg	$h_{turbine\ inlet} - h_{turbine\ outlet}$	(4)
Q_{in}	kJ/kg	$h_{heater\ outlet} - h_{heater\ inlet}$	(5)
W_{specific}	kJ/kg	$\frac{\sum W_{expansion} - \sum W_{compression}}{\dot{m}}$	(6)
η_{thermal}	–	$\frac{\sum W_{expansion} - \sum W_{compression}}{\sum Q_{in}}$	(7)
X_{split}	–	$\frac{\dot{m}_{cooler}}{\dot{m}}$	(8)

5. Model Validation

To ensure the model accuracy, validation is carried out in two parts, first part validating a cycle with pure CO_2 while the second validation is with CO_2/R152a mixture.

5.1. Pure CO_2

The data present in [52] study is used for validation. The simulation results are listed in Table 7. The calculated cycle efficiency, as shown in the table, shows good agreement with the results of reference, with <1 % difference. The difference in the modeling software as well as the equation of state may account for this difference.

5.2. CO_2/R152a mixture

A trans-critical power cycle from [53] study will be used for validation of CO_2/R152a. Results calculated in this study are listed in Table 8. They are in good agreement with the reference results, which validates the method used and the calculated mixture properties.

6. Response surface method

Response surface method (RSM) is a combination of statistical experimental design, regression techniques, and optimization methods used to identify and relate experimental data in a good-fitting response model to relate output or multiple outputs with multiple decision/input variables. The input for this technique is in the form of experimental design which was carried in Minitab software. The experimental design used in this study is a full factorial design. As an output, a regression equation for the calculation of the response variable is generated and tested [54]. The equation will help in determining optimum parameters values for the maximum output [55].

To determine the most significant input variables, analysis of variance (ANOVA) based on the experimental results is carried out and p and F values are assigned to each variable to determine the significance score. Moreover, the accuracy of the regression model is assessed using R^2 and adjusted R^2 values, the values of these variables are recommended to be closer to 1 for best fit of the regression model.

In this study, 4 independent parameters are considered. Namely, additive molar fraction (F_{mol}), cycle minimum temperature ($T_{\min}$), turbine expansion pressure (P_{exp}) and split ratio (X_{split}). Each factor is analyzed at 3 levels as. The limits and levels are presented in Table 9. Based on the selected variables, number of cycles and the mixtures considered in this study, a total number of 252 experimental runs are carried out. However, few runs are excluded, where the required MITA value wasn't achievable in the recuperator. All the experimental runs to prepare a full factorial matrix are performed in Aspen Plus simulation environment.

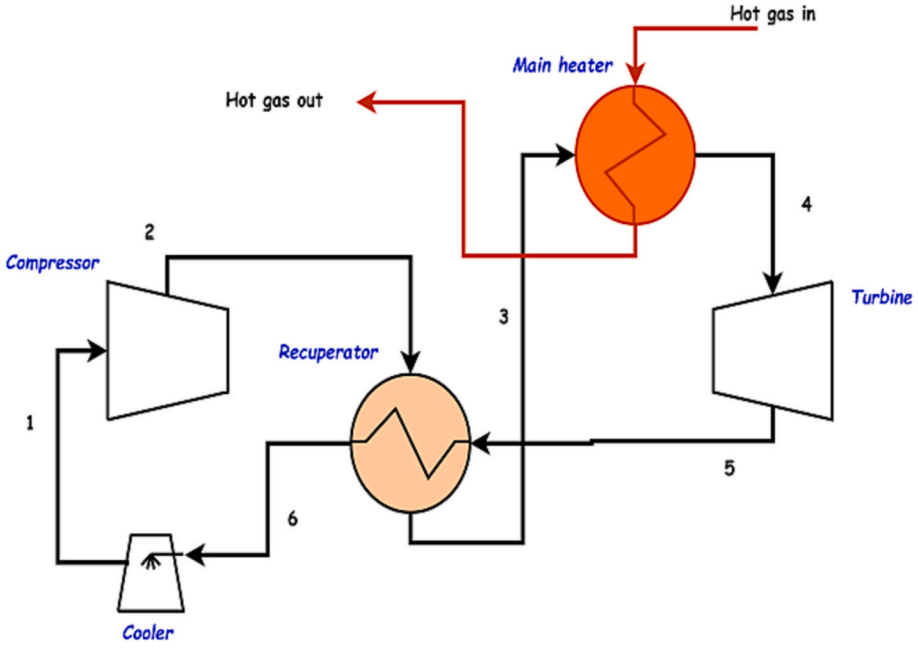

Fig. 5. Simple recuperated cycle.

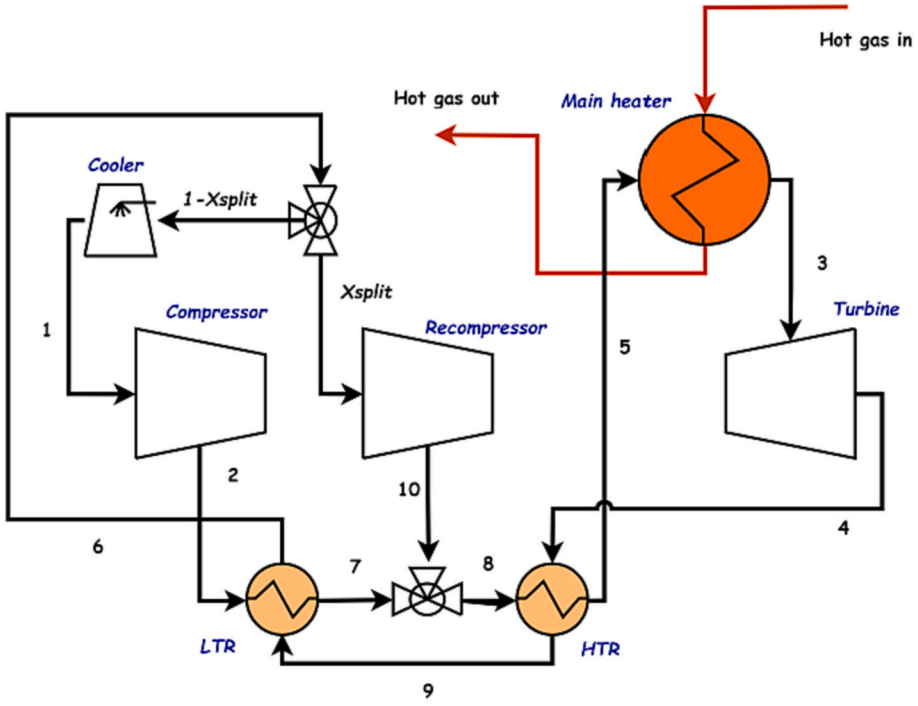

Fig. 6. Recompression cycle.

7. Multiobjective genetic algorithm

After single-objective optimization using RSM method, a multi objective optimization is carried out. Multi-objective genetic algorithm is an optimization technique that involves solving multiple objectives simultaneously. The MOGA uses a population of candidate solutions to search for optimal solutions. It iteratively generates possible solutions through selection and mutation.

The possible candidates are evaluated based on their fitness to the objectives of the problem. The fittest candidates are shortlisted and evaluated again. The process will be applied repeatedly until a satisfactory set of solutions is achieved. MOGA can be used to find a set of solutions that are optimal with respect to all these objectives. It can also handle problems with multiple constraints and can find solutions that are robust to changes in the problem parameters. Most importantly, it represents possible solutions that include tradeoffs between conflicting objectives, which is not possible in single-objective optimization.

The Pareto front is used to represent the set of optimal solutions. A Pareto front is a set of nondominant solutions that cannot be improved in any of the objectives without degrading any of the other objectives. The set of all such solutions that are non-dominated constitutes the Pareto front. It provides deeper insights into the trade-off among the

Table 6
Input parameters for power cycles simulations.

Parameters	Units	Values
Product gas temperature, T_{gas}	°C	500
Turbine inlet temperature, T_{max}	°C	450
Turbine expansion pressure, P_{exp}	MPa	8–10
Compressor inlet temperature, T_{min}	°C	40–65
Maximum cycle pressure, P_{max}	MPa	25
Turbine isentropic efficiency, $\eta_{T,ise}$	–	0.92
Compressor isentropic efficiency, $\eta_{C,ise}$	–	0.88
Mechanical efficiency, η_{mech}	–	0.97
Recuperator minimum temperature approach, *MITA*	°C	15
Mass flow split ratio, X_{split}	–	0.6–0.8

Table 7
Thermodynamic model validation for pure CO_2.

Parameter	Value	Unit
Cycle efficiency (This work)	41.3	%
Cycle efficiency (Reference [52])	40.9	%
Percentage Difference	0.96	%

Table 8
Thermodynamic model validation for CO_2/R152a mixture.

Parameter	Value	Unit
Molar Fraction CO_2/R152a	0.5/0.5	–
Cycle efficiency (This work)	35.6	%
Cycle efficiency (Reference [53])	35	%
Percentage Difference	1.58	%

Table 9
Decision factors and their levels for full factorial design.

Factors	Unit	Minimum level	Intermediate level	Maximum level
Compressor inlet temperature, T_{min}	°C	40	52.5	65
Turbine expansion pressure, P_{exp}	MPa	8	9	10
Flow split ratio, X_{split}	–	0.6	0.7	0.8
Percentage mole fraction, F_{mol}	R152a	5	10	15
	C_6H_6	1	2.3	3.6

objectives and helps to identify the best solution among the Pareto front solutions.

In this study, cycle thermal efficiency and cycle specific work are set as the objectives for the multi-objective optimization within the same bounds used in RSM. The regression equations that are generated through the design of experiments are used as the objective functions.

8. Regression analysis

The following polynomial equation is used to fit independent parameters and responses to the experiment's results.

$$Y = B_0 + \sum_{i=1}^{k} B_i x_i + \sum_{i=1}^{k} B_{ij} {x_i}^2 + \sum_{i=1}^{k-1} \sum_{j=2}^{k} B_{ij} x_i x_j \quad (9)$$

where Y denotes the anticipated outcome or performance indicator. B_o, B_i, B_{ii}, and B_{ij} are the assigned constant, linear, quadratic, and interaction regression coefficient values, respectively. I and j are index numbers, whereas Xi and Xj are the input parameters. The regression equation that results computes the influence of the input variables and their interactions based on experiments listed in Appendix-A. The mathematical models of the cycle efficiency and cycle specific work of both mixtures and the two types of cycle configurations are derived as a result of regression analysis are recorded in Appendix B.

8.1. Regression model accuracy

The previous thermodynamic results are used to fit a regression equation of each case separately. The accuracy of the models is represented in the form of R^2, adjusted R^2 and predicted R^2. Their values range from 1 to 100. The closer the value is to 100, the more accurate the model is. Table 10 shows values above 93 reflecting the high accuracy of the models.

8.2. Analysis of variance (ANOVA)

By applying ANOVA analysis on the simulation results, the significance of varied variables on thermal efficiency and cycle specific work is investigated. *P* values below 0.05 reflect high significance and the F value is also a measure of the significance where higher F value means higher significant variable. In simple recuperated cycle, cycle minimum temperature is the most significant parameter followed by molar fraction for both R152a-CO_2 and C_6H_6-CO_2 mixtures as represented in Table 11. (See Table 12.)

While for recompression cycle most significant parameter is cycle minimum temperature followed by split mass fraction based on their high F-value.

9. Results and discussion

In this section, a sensitivity analysis is performed to determine the effect of the significant cycle parameters (decided in the previous section) on the cycle efficiency. The purpose of these charts is to select the optimum operating range that yields the highest cycle efficiency and cycle-specific work, as well as to find the cycle configuration that is less sensitive to variations in cycle decision parameters.

9.1. Analysis of cycle efficiency

9.1.1. Influence of mixture composition and compressor inlet temperature

The study of the increase in compressor inlet temperature (or cycle minimum temperature) is important because this temperature is directly affected by the increase in air temperature in the dry cooler of the power cycle under hot ambient temperature conditions. The effect of increase in compressor inlet temperature and mixture composition is shown in Fig. 7 and Fig. 8 for CO_2-R152a and CO_2-C_6H_6 mixtures respectively. From the contours of cycle layouts with CO_2-R152a mixture, it is observed that the increase in additive molar fraction allows for achieving higher efficiency over a wider range of the cycle minimum temperature. At a cycle minimum temperature of 50 °C, the efficiency increases by 1 point from 31 to 32% in the simple cycle, with an increase in the molar fraction from 5 to 15%, while the compression work reduces from 55 kW to 36 kW. While for the recompression cycle, at the same cycle minimum temperature, efficiency increases by approximately 3 points from 31.7 to 34.5% with the increase of molar fraction from 5 to 15% and the total compression work changes from 66 kW to

Table 10
Accuracy ratings of fitted regression models.

Cycle	Parameter	Additive	R^2	R^2 Adj	R^2 Pred
Simple Recuperated	Cycle specific work	R152a	97.6	96.33	93.71
		C_6H_6	98.05	97.01	93.99
Simple Recuperated	Cycle efficiency	R152a	98.75	98.09	96.43
		C_6H_6	99.04	98.53	97.53
Recompression	Cycle specific work	R152a	97.48	96.87	95.71
		C_6H_6	98.63	98.25	97.57
Recompression	Cycle efficiency	R152a	96.81	96.04	94.54
		C_6H_6	97.99	97.43	96.39

Table 11
Analysis of variance of simple recuperated cycle.

Source	Cycle efficiency [%]				Cycle specific work [kJ/kg]			
	CO_2-R152a		CO_2-C_6H_6		CO_2-R152a		CO_2-C_6H_6	
	F-Value	*P*-Value	F-Value	P-Value	F-Value	P-Value	F-Value	P-Value
Model	149.56	0	194.6	0	76.76	0	94.74	0
Linear	425.64	0	555.83	0	218.03	0	276.41	0
F_{mol}	49.79	0	29.2	0	29.13	0	33.07	0
T_{min}	1224.49	0	1621.27	0	579.11	0	780.94	0
P_{exp}	2.64	0.123	17.04	0.001	45.84	0	15.22	0.001
2-Way Interaction	19.72	0	25.37	0	11.47	0	3.68	0.033
F_{mol}*T_{min}	8.29	0.01	3.22	0.091	2.87	0.109	0.82	0.378
F_{mol}*P_{exp}	2.15	0.161	6.11	0.024	5.41	0.033	4.21	0.056
P_{exp}*T_{min}	48.72	0	66.78	0	26.12	0	6	0.025

Table 12
Analysis of variance of recompression cycle.

Source	Cycle efficiency [%]				Cycle specific work [kJ/kg]			
	CO_2-R152a		CO_2-C_6H_6		CO_2-R152a		CO_2-C_6H_6	
	F-Value	P-Value	F-Value	P-Value	F-Value	P-Value	F-Value	P-Value
Model	125.77	0	174	0	160	0	257.85	0
Linear	412.95	0	456.52	0	516.12	0	706.47	0
F_{mol}	134.92	0	100.63	0	188.82	0	181.56	0
T_{min}	1569.75	0	1669.81	0	1720.4	0	2148.02	0
P_{exp}	118.15	0	222.76	0	1.78	0.188	68.91	0
X_{split}	266.83	0	408.04	0	402.14	0	624.17	0
2-Way Interaction	23.34	0	23.05	0	14.74	0	9.4	0
F_{mol}*T_{min}	23.97	0	4.32	0.043	5.47	0.023	0.17	0.684
F_{mol}*P_{exp}	27.17	0	15.64	0	30.24	0	24.86	0
F_{mol}*X_{split}	15.02	0	8.65	0.005	4.27	0.043	1.42	0.239
P_{exp}*T_{min}	62.67	0	24.7	0	64.82	0	20.75	0
X_{split}*T_{min}	78.43	0	120.67	0	7.82	0.007	11.21	0.002
P_{exp}*X_{split}	17.66	0	28.18	0	15.01	0	23.52	0

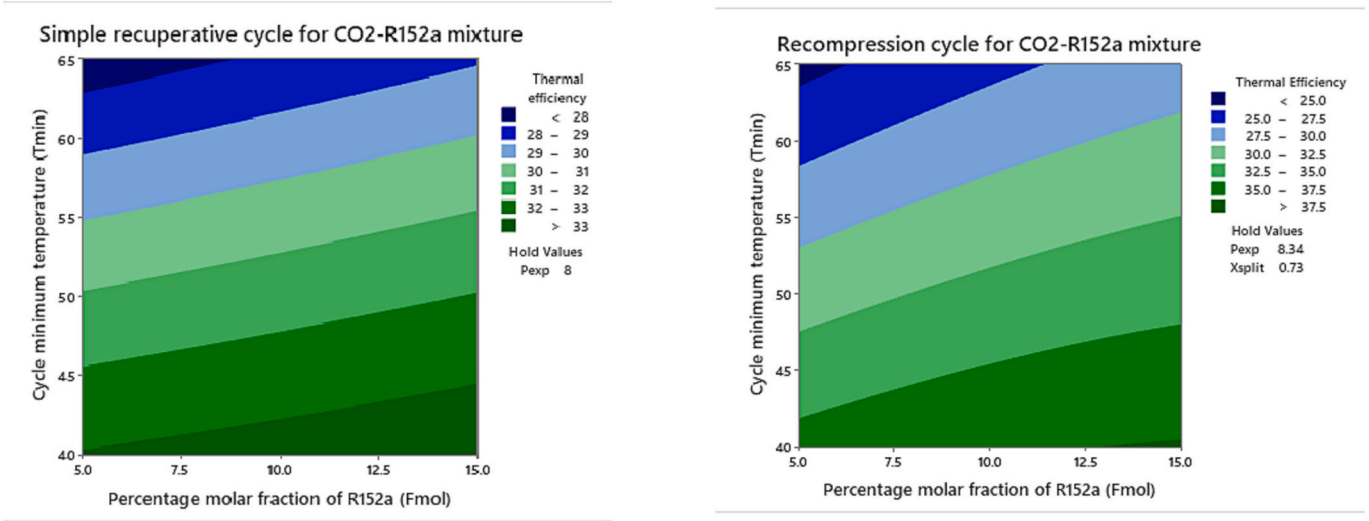

Fig. 7. Contours of cycle efficiency subject to rise in cycle minimum temperature and increase in molar fraction of additive R152a in mixture operating in simple and recompression cycle configurations.

45 kW.

For the CO_2-C_6H_6 mixture, the increase in the additive molar fraction also results in higher efficiency for the same cycle minimum temperature. For simple cycle, at 48 °C cycle minimum temperature, efficiency increases by up to 1 point from 30.9 to 31.7%, with the increase of molar fraction from 1 to 3.6%. The increase in efficiency is the manifestation of a decrease in the compression work from 57 kW to 48.5 kW. The recompression cycle, on the other hand, has an efficiency gain of 2.4 points, from 30.5 to 32.9%, with a molar fraction increase of 1 to 3.6% at the cycle minimum temperature of 48 °C whereas total compression work decreases from 52 kW to 42 kW.

Overall, the CO_2-R152a mixture with a 15% molar fraction of R152a exhibits superior performance compared to the CO_2-C_6H_6 mixture in the range of composition considered in this work. Moreover, among the considered cycle configurations, the recompression cycle demonstrates better performance. Moreover, the cycle layout, which is more sensitive

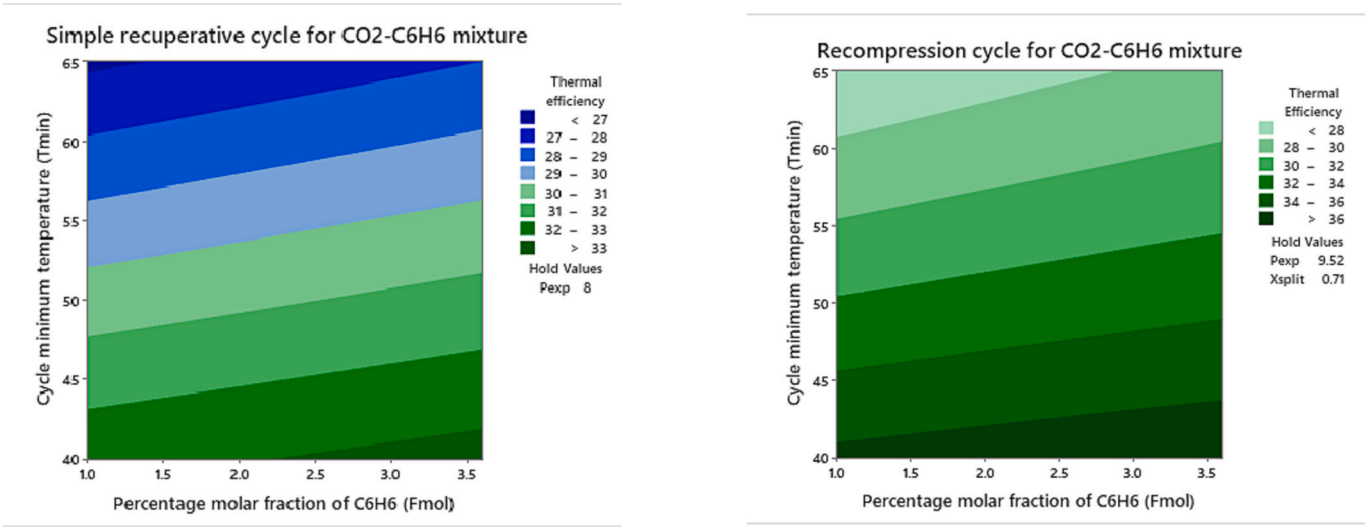

Fig. 8. Contours of cycle efficiency subject to rise in cycle minimum temperature and rise in molar fraction of the additive C_6H_6 in the mixture operating in simple and recompression cycle configurations.

to an increase in the cycle minimum temperature, is a recompression cycle compared to a simple cycle configuration for a fixed molar fraction of the additive.

9.1.2. Influence of mixture composition and turbine expansion pressure

The turbine inlet pressure is fixed at state-of-the-art value of 25 MPa, still there can be changes in turbine outlet pressure during part load operation of the power cycle. Therefore, it is also important to investigate the effect of the change in turbine outlet pressure from 8 to 10 MPa on the cycle efficiency.

For both the mixtures, at higher turbine expansion pressures (P_{exp} > 9 MPa), No significant improvement in cycle efficiency is noticed with rise in mixture composition (See Fig. 9 and Fig. 10). For instance, in the case of the recompression cycle with CO_2-R152a mixture, an increase by >2 points in thermal efficiency from 35.3 to 37.6% and a decrease of 11 kW in total compression work with the molar fraction increase from 5 to 15% is observed at an expansion pressure of 8 MPa. At an expansion pressure of 9.5 MPa, with molar fraction increase, efficiency increases from 37% to 37.5% and total compression work decreased. A slight decrease in efficiency is observed at an additive molar fraction above 12%.

Similarly, for the CO_2-C_6H_6 mixture in the recompression cycle layout, at 8 MPa expansion pressure with the molar fraction increasing from 1 to 3.6%, an increase of 2 points in thermal efficiency from 34% to 36%, along with a decrease in compression work from 67 kW to 51 kW. While, for 9.5 MPa, an increase by half point from 36% to 36.5% efficiency is observed while increasing the additive molar fraction.

9.1.3. Influence of mixture composition and mass split fraction

The impact of the mass split fraction on the recompression cycle's efficiency is significant, and identifying the optimal range of split fractions corresponding to different molar fractions is crucial. Fig. 11 demonstrate the effect of an increase in split fraction and additive molar fraction in the mixture on cycle efficiency for the two mixtures under consideration.

The efficiency contour of the CO_2-R152a mixture and calculations show that at a split of 0.65, efficiency increases from 34.3% to 37.1% (~3 points) and total compression work decreases from 43 kW to 35 kW with the increase of molar fraction from 5 to 15%. Similarly, at a split of 0.8, efficiency increases from 36% to 37.1% (~1 point) and total compression work reduces by 6 kW with the same increase in molar fraction. In contrast, the CO_2-C_6H_6 mixture's contour shows that at a

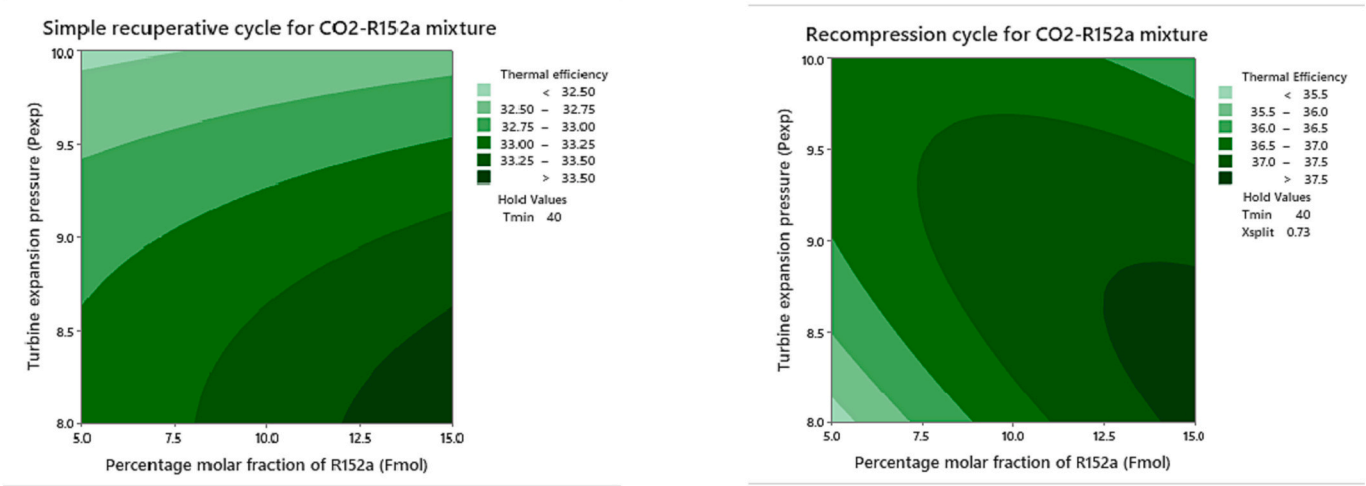

Fig. 9. Contours of cycle efficiency subject to rise in turbine expansion pressure and rise in molar fraction of the additive R152a in the mixture operating in simple and recompression cycle configurations.

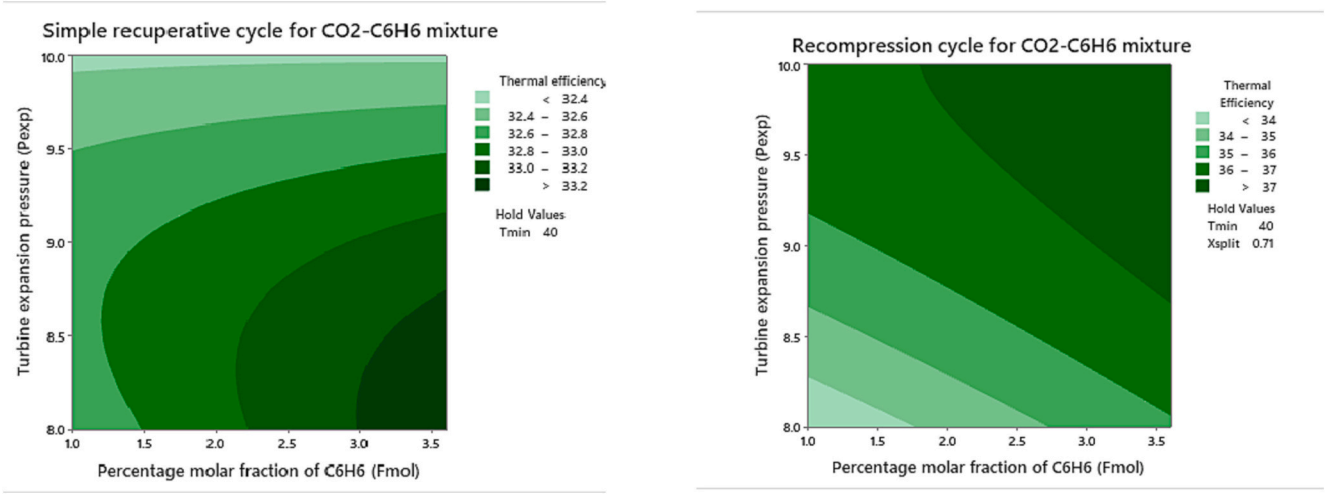

Fig. 10. Contours of cycle efficiency subject to rise in turbine expansion pressure and rise in molar fraction of the additive C_6H_6 in the mixture operating in simple and recompression cycle configurations.

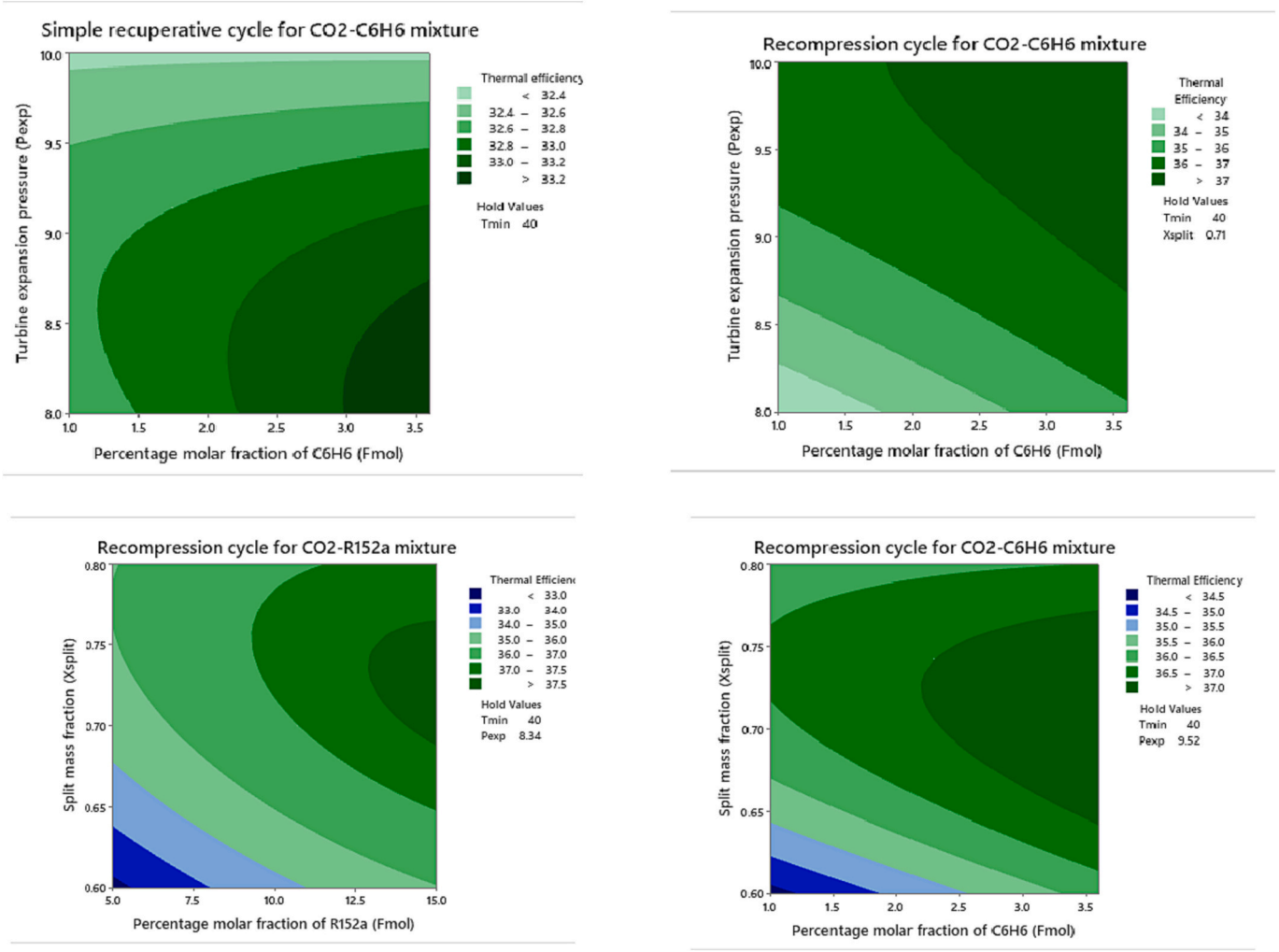

Fig. 11. Contours of cycle efficiency subject to rise in split mass fraction and rise in molar fraction of the additive in the mixture operating in recompression cycle configuration.

split of 0.65, efficiency increases from 35.6% to 37.1% (1.5 points) and total compression work decreases from 43.7 kW to 38 kW. While at a split of 0.8, efficiency increases from 36% to 36.5% (0.5 point) and total compression work decreases by 5 kW with the increase of additive molar fraction from 1% to 3.6%.

Furthermore, it is observed that as the additive's composition in both

mixtures increases, the cycle efficiency becomes less sensitive to the change in split mass fraction. In the CO_2-R152a mixture, at 5% molar fraction, efficiency increases from 32.7% to 36% (~3 points) when increasing the split ratio from 0.6 to 0.8, while the increase in split ratio results in 1 point increase in efficiency at 15% molar fraction. Similarly, for the CO_2-C_6H_6 mixture, at 1% molar fraction, efficiency varies by a maximum of 2 points when increasing the split ratio from 0.6 to 0.8. At 3.5% molar fraction, the efficiency varies by a half point for the same split ratio range.

To understand the relation between mass split and efficiency, LMTD of the low-temperature recuperator and recompression work are compared at different mass splits. For CO_2-R152a mixture, with constant variable values set to cycle minimum temperature of 40 °C, molar fraction of 7.5% and expansion pressure of 8.34 MPa. At a mass split of 0.65, LMTD of LTR is 20.9 °C and recompression work is 28 kW, which is decreased with a split of 0.8 to16.5 °C and 15 kW respectively. Similarly, for CO_2-C_6H_6 mixture, and setting cycle minimum temperature to 40 °C, molar fraction of 3% and expansion pressure of 9.5 MPa. At a split of 0.65, LMTD of LTR is 18.9 °C and recompression work is 22.3 kW, which is decreased to12°C and 11.6 kW respectively at the split fraction of 0.8. Variations in mass split are directly influencing LMTD of LTR and recompression work which explains the change in the cycle efficiency.

Overall, when using the CO_2-R152a mixture, maximum efficiency is achieved in the split ratio range of 0.65 to 0.8, at a molar fraction above 10%. But when using the CO_2-C_6H_6 mixture, it is achieved in the split ratio range of 0.65 to 0.76, at a molar fraction above 2.2%.

9.2. Analysis of cycle specific work

9.2.1. Influence of mixture composition and compressor inlet temperature

Another performance parameter considered is cycle specific work; as the study focuses on heat recovery applications, cycle specific work is of high importance. In Fig. 12 and Fig. 13, a similar trend as in efficiency is visible where the increase in molar fraction results in the increase in cycle specific work of the cycle. For the CO_2-R152a mixture in the simple cycle, cycle specific work is found to be increasing from 68.9 kJ/kg to 74 kJ/kg at a minimum temperature of 55 °C, while varying additive composition from 7% to 12%. Also, the compression work decreases from 56.8 kW to 50 kW. On the other hand, in the recompression cycle, the increase in cycle specific work is by 5 kJ/kg from 55 kJ/kg to 60 kJ/kg with the change in molar fraction from 7 to 12%. And the total compression work decreases from 68.5 kW to 61.9 kW.

In the case of the CO_2-C_6H_6 mixture, at a fixed minimum temperature of 50 °C, the increase in molar fraction from 1 to 3% resulted in a 4.5 kJ/kg increase in cycle specific work output in the case of simple cycle accompanied by a decrease in compression work from 58.5 kW to 52.6 kW. While an increase of cycle specific work by 4.5 kJ/kg with a decrease in compression work by 6 kW in the recompression cycle. Detail is presented in Figs. 14-16.

At higher minimum cycle temperatures, the operating conditions of the cycle are away from the critical point of the mixture, which results in increased compression work thus affecting the performance of the cycle, but with the increase in molar fraction, the gap reduces resulting in a better cycle performance as evident from the results.

9.2.2. Influence of mixture composition and turbine expansion pressure

Next is the comparison of the effect of varying turbine expansion pressure and the molar fraction on the cycle specific work. Using the CO_2-R152a mixture, in the simple cycle at a low expansion of 8.5 MPa, cycle specific work is found to be increasing from 86.4 kJ/kg to 88.7 kJ/kg, while varying additive composition from 7% to 12%. At same expansion pressure, the recompression cycle shows an increase in cycle specific work from 76.8 kJ/kg to 80.6 kJ/kg with the change in molar fraction from 7 to 12%. The increase in cycle specific work is because of the decrease in the compression work due to the increased molar fraction.

In the case of the CO_2-C_6H_6 mixture in the simple cycle, at a fixed expansion pressure of 8.5 MPa, the increase in the molar fraction from 1 to 3% resulted in an rise in cycle specific work from 82.1 to 87.4 kJ/kg with a decrease of 9 kW in compression work.

Also, in the recompression cycle, at a fixed expansion pressure of 8.5 MPa, the increase in molar fraction from 1 to 3% resulted in an increase in cycle specific work from 70.9 to 77.1 kJ/kg and a decrease in total compression work by 12.5 kW.

9.2.3. Influence of mixture composition and mass split fraction

To study the influence of mass split ratio and additive molar fraction on the cycle specific work, study of their effect is performed while the optimum values of other parameters are held constant. In cycle with R152a additive composition varied from 7 to 12%, at a mass split of 0.65, cycle specific work increased from 66.8 kJ/kg to 72.7 kJ/kg as compared to increase from 74.3 kJ/kg to 79.4 kJ/kg at a mass split of 0.75. At same conditions, total compression work varied by 8 kW at a mass split of 0.65 while varied by 7 kW at mass split of 0.75.

In the other case with C_6H_6 additive composition varied from 1 to 3%, at a mass split of 0.65, Compression work decreased by 13 kW and cycle specific work increased by 7 kJ/kg from 61.1 kJ/kg to 68.1 kJ/kg as compared to compression work decreased by 11 kW and cycle specific

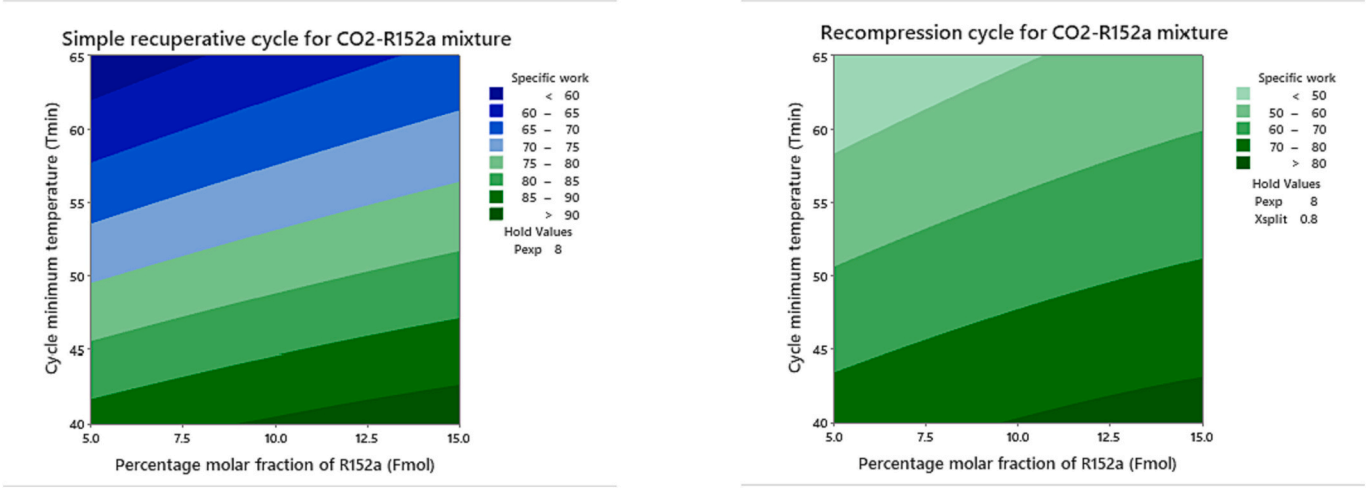

Fig. 12. Contours of cycle specific work subject to rise in cycle minimum temperature and rise in molar fraction of the additive R152a in the mixture operating in simple and recompression cycle configurations.

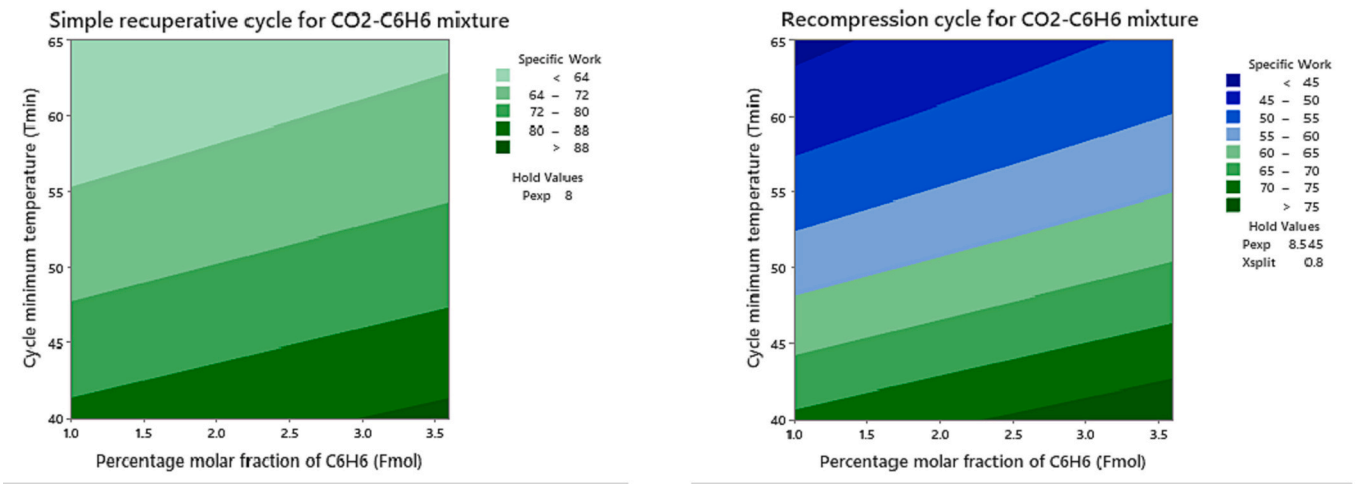

Fig. 13. Contours of cycle specific work subject to rise in cycle minimum temperature and rise in molar fraction of the additive C_6H_6 in the mixture operating in simple and recompression cycle configurations.

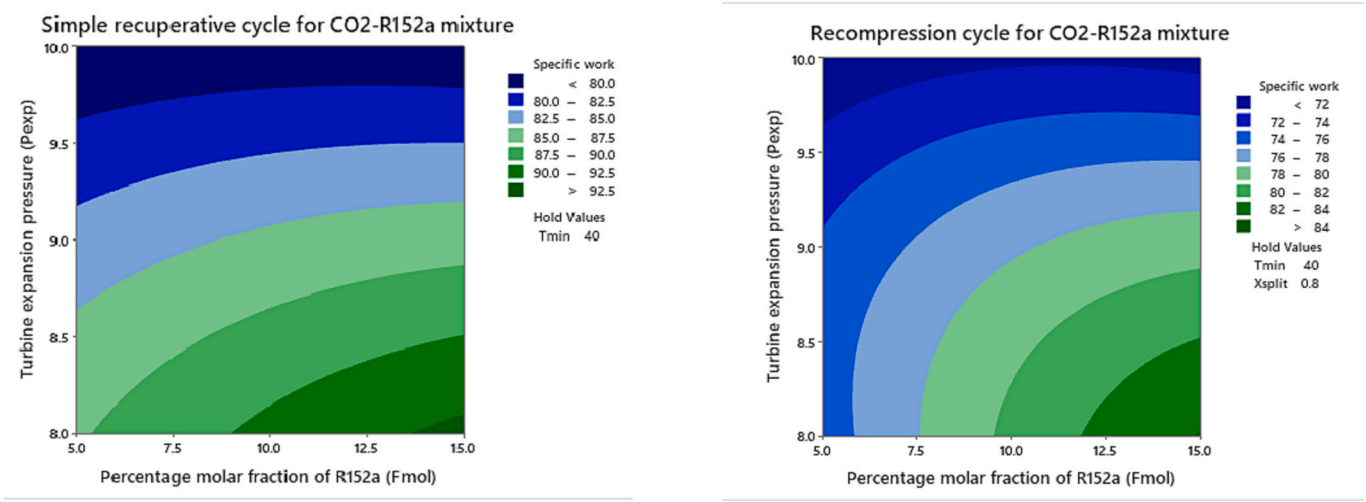

Fig. 14. Contours of cycle specific work subject to rise in turbine expansion pressure and rise in molar fraction of the additive R152a in the mixture operating in simple and recompression cycle configurations.

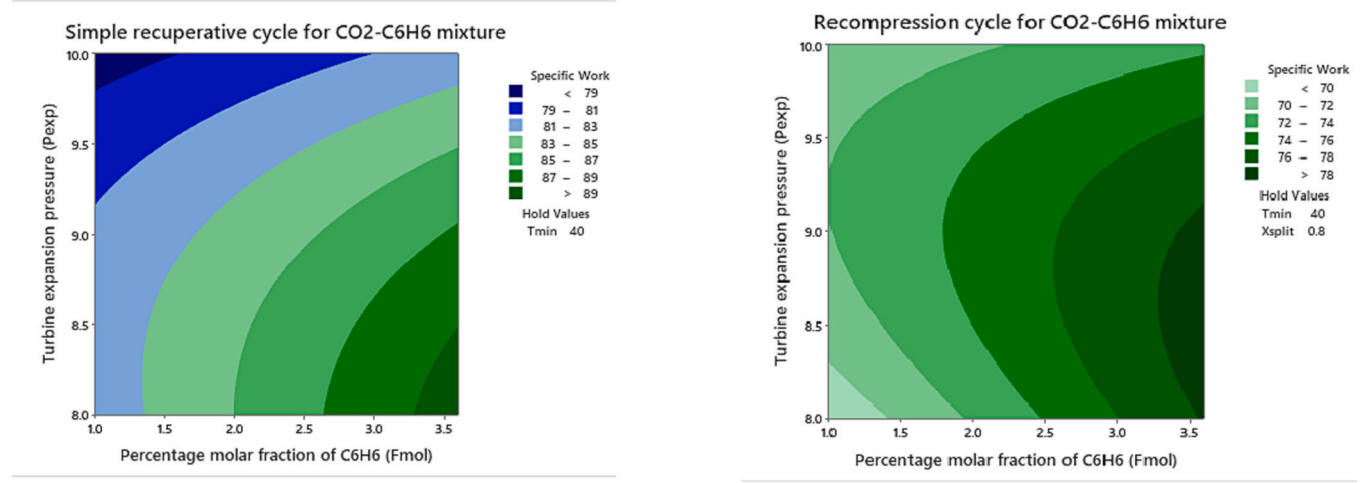

Fig. 15. Contours of cycle specific work subject to rise in turbine expansion pressure and rise in molar fraction of the additive C_6H_6 in the mixture operating in simple and recompression cycle configurations.

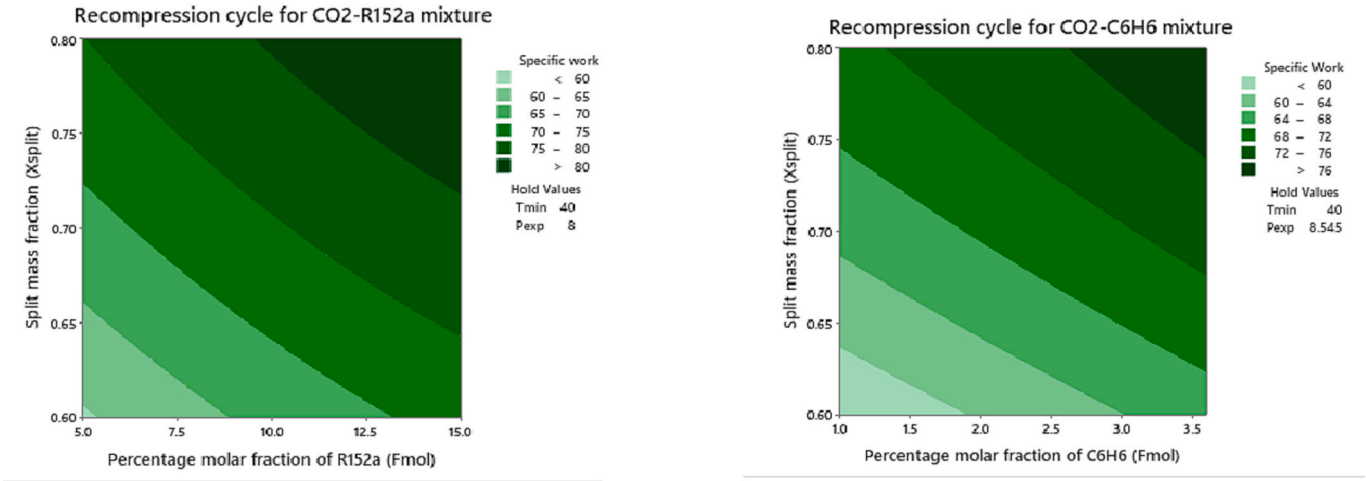

Fig. 16. Contours of cycle specific work subject to rise in split mass fraction and rise in molar fraction of the additive in the mixture operating in recompression cycle configuration.

work increase by 6 kJ/kg from 68.3 kJ/kg to 74.3 kJ/kg at a mass split of 0.75. Overall, higher mass split shows higher cycle specific work in both mixtures.

Further analysis on the LMTD of a low-temperature recuperator and recompression work is needed to understand the response to change in mass split. Beginning with CO_2-R152a mixture, with constant variable values set to minimum temperature of 40 °C, molar fraction of 7.5% and expansion pressure of 8.34 MPa. At a mass split of 0.65, recompression work is 28 kW and LMTD of LTR is 20.9 °C, which is decreased with a split of 0.8 to 15 kW and 16.5 °C respectively. Similarly, for CO_2-C_6H_6 mixture, and setting minimum temperature to 40 °C, molar fraction of 3% and expansion pressure of 9.5 MPa. At a split of 0.65, LMTD of LTR is 18.9 °C and recompression work is 22.3 kW, which is decreased with a split of 0.8 to 12 °C and 11.6 kW respectively. It is noted that variations in mass split are directly influencing LMTD of LTR and recompression work which explains the change in the cycle specific work as well as in the efficiency.

It is clear from the results that with respect to cycle specific work, the simple cycle is better performing among the two cycle configurations which are different from the results with respect to cycle efficiency. However, in both cases, higher performance is achieved by CO_2-R152a mixture in the considered range of molar fraction.

9.3. Multi-objective genetic algorithm optimization

The analysis carried out in previous sections using RSM help identify the behavior of cycle efficiency and cycle specific work individually while varying two parameters at a time. This helps in identifying the optimal ranges of those variables. However, it doesn't provide an optimal point of all studied variables together. Also, both objectives as clear in contours, have different tendencies of optimal ranges in the recompression cycle. Therefore, multi-objective optimization is carried out to find the exact optimal point of each mixture for achieving both objectives together.

The regression equations generated in the analysis in preceding sections are used as objective functions in multi objective optimization for maximum efficiency and cycle specific work.

Objective function	$max\eta$ $and max w$
Constraints	$5 \leq F_{mol} \leq 15$ (R152a) $1 \leq F_{mol} \leq 3.6$ (C_6H_6) $40 \leq T_{min} \leq 65$ $8 \leq P_{exp} \leq 10$ $0.6 \leq X_{split} \leq 0.8$

Complete Pareto front values are listed in Appendix C. The results of the recompression cycle for CO_2-R152a mixture in Pareto front represented in Fig. 17 show a variation of results between achieving a maximum cycle specific work, maximum efficiency or a point in between based on trade-offs. The maximum efficiency point has a cycle specific work of 80 kJ/kg and efficiency of 37.7%. And the maximum cycle specific work point is at 83.9 kJ/kg with an efficiency of 37.2%. The middle point is at cycle specific work of 82.4 kJ/kg and efficiency of 37.5%. As the study is based on heat recovery application, achieving maximum cycle specific work is desired. The optimum values of studied parameters should be, 14.8% additive molar fraction, 40 °C minimum temperature, 8.01 MPa expansion pressure and a split of 0.79.

For CO_2-C_6H_6 mixture in recompression cycle, the maximum efficiency point has a cycle specific work of 74.5 kJ/kg and efficiency of 37.4%. And the maximum cycle specific work point is at 78.8 kJ/kg with an efficiency of 36.6%. The middle point is at cycle specific work of 76.8 kJ/kg and efficiency of 37.2%. To achieve maximum cycle specific work, the optimum values of studied parameters should be, 3.59% additive molar fraction, 40 °C cycle minimum temperature, 8.75 MPa expansion pressure and a split of 0.79.

9.4. Comparative analysis with pure CO_2 supercritical power cycle

To determine the improvements in cycle specific work attained by using CO_2-based mixtures instead of supercritical pure CO_2 power cycles, we conducted a comparative analysis of both cycle configurations. Optimal values for each mixture and pure CO_2 are obtained through thermodynamic evaluation and statistical analysis as explained in previous sections. The comparison is conducted at varying cycle minimum temperatures while maintaining other parameters at their optimal values. This allowed us to assess the potential benefits of utilizing mixtures as working fluids in supercritical power cycles under harsh climate conditions.

Fig. 18 and Fig. 19 illustrate the comparison of cycle specific work for the simple and recompression cycle configurations, respectively. In the simple recuperative cycle configuration, the use of the CO_2-R152a mixture resulted in an average increase of 13 kJ/kg in cycle specific work compared to the sCO_2 power cycle. Similarly, the CO_2-C_6H_6 mixture showed an average of 9 kJ/kg gain in cycle specific work. In recompression cycle, the CO_2-R152a mixture showed an average of 12 kJ/kg increase in cycle specific work, and the CO_2-C_6H_6 mixture showed an average of 7.5 kJ/kg increase. Overall, the CO_2-R152a mixture showed better results in both cycle configurations, compared to the pure CO_2 power cycle with simple cycle having maximum achieved cycle

specific work.

10. Conclusion

This study aimed to investigate the potential benefits of using CO_2-based mixtures as working fluids in supercritical power cycles. Sensitivity of cycle efficiency and cycle specific work is performed towards increase in additive molar fraction, increase in cycle minimum temperature, increase in turbine expansion pressure and variation in split mass fraction. Main novelty of this works lies in the use of response surface method (RSM) to derive objective functions of cycle efficiency and cycle specific work. The use of RSM allows to study the simultaneous effect of two variables at a time on cycle thermodynamic performance. It provides objective functions with acceptable accuracy for study of cycle performances subject to variation in several decision variables.

From the thermodynamic analysis and comparative study, the following conclusions can be drawn:

1. The cycle performance of mixtures is improving with increase in additive molar fraction in the mixture. The CO_2-R152a mixture showed larger cycle efficiency and higher cycle specific work among the considered mixtures and within the considered range of compositions.
2. The rise in cycle minimum temperature, keeping turbine expansion pressure at optimum value brings about a significant decrease in cycle efficiency. The maximum variation in the cycle efficiency with rise in cycle minimum temperature is observed in the recompression cycle which makes it the most sensitive configuration towards rise in cycle minimum temperature.
3. The increase in expansion pressure shows higher sensitivity of cycle specific work as compared to the effect on cycle efficiency.
4. Varying the split mass fraction has a significant impact on the efficiency as well as cycle specific work of the recompression cycle. As the additive's composition in both mixtures increases, the cycle efficiency and specific work become less sensitive to changes in the split mass fraction. However, the optimal ranges of mass split vary between both objectives. The CO_2-R152a mixture achieves maximum efficiency in the split ratio range of 0.65 to 0.8, at a molar fraction above 10%, while the CO_2-C_6H_6 mixture achieves maximum efficiency in the split ratio range of 0.65 to 0.76, at a molar fraction above 2.2%. On the other hand, CO_2-R152a mixture achieves maximum cycle specific work at a split above 0.72 and molar fraction above 10%. CO_2-C_6H_6 mixture achieves maximum specific work at a split above 0.74 and molar fraction above 2.5%.
5. In the simple recuperated cycle, the maximum cycle performance is achievable for both objectives combined. For the CO_2-R152a mixture, a maximum specific power of 92.5 kJ/kg and efficiency of 33.6% are achieved at a minimum temperature of 40.1 °C, additive molar fraction of 14.75%, and expansion pressure of 8 MPa.
6. In the recompression cycle, a tradeoff is necessary between the cycle specific work and efficiency, a maximum specific work of 83.9 kJ/kg and corresponding efficiency of 37.2% are achieved using CO_2-R152a mixture at a minimum temperature of 40 °C, additive molar fraction of 15%, expansion pressure of 8 MPa and a split ratio of 0.8.
7. Comparative analysis demonstrates improved cycle specific work of CO_2-based mixtures compared to the supercritical pure CO_2 power cycle in the two cycle configurations. For the recompression cycle configuration with the optimum composition of the CO_2-R152a mixture resulted in an average 12 kJ/kg increase in cycle specific work compared to the pure CO_2 power cycle, while the CO_2-C_6H_6 mixture showed 7.5 kJ/kg increase. However, a higher average gain

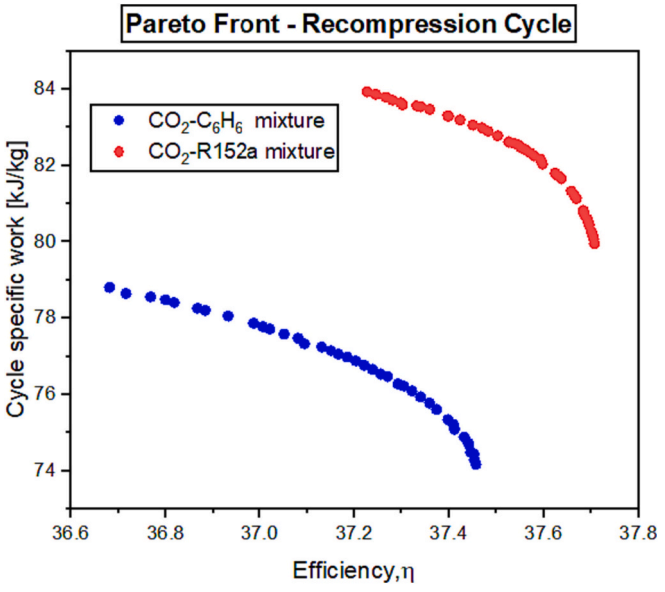

Fig. 17. Pareto front of efficiency and specific work of recompression cycle.

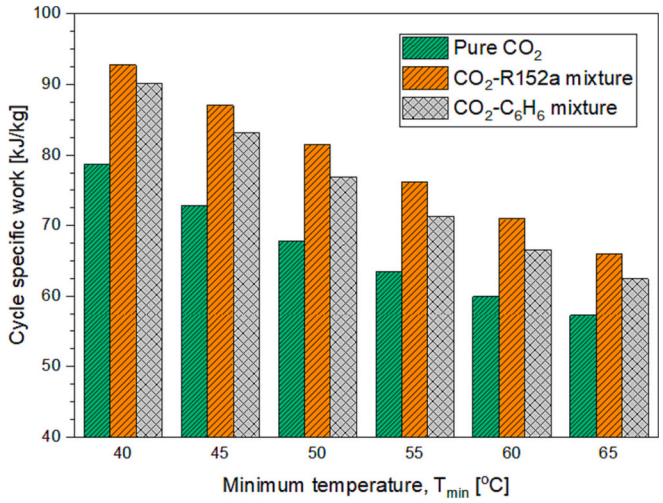

Fig. 18. Mixture's specific work comparison at optimum values for simple recuperated cycle.

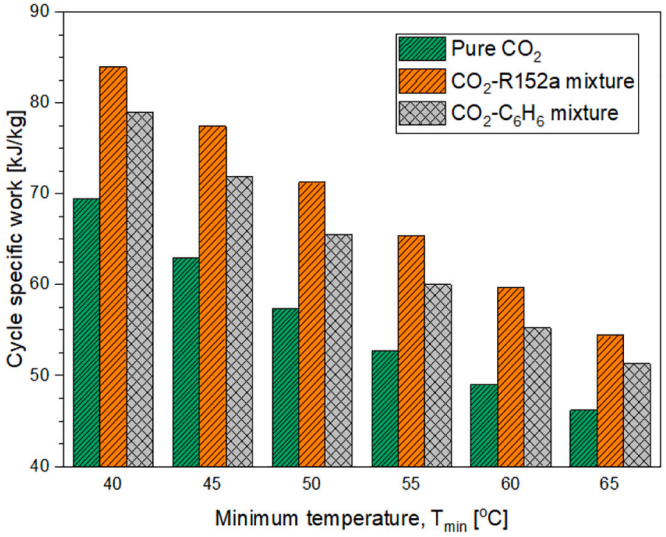

Fig. 19. Mixture's specific work comparison at optimum values for recompression cycle.

in cycle specific work is observed in the simple recuperated cycle configuration, where the CO_2-R152a mixture showed 13 kJ/kg increase, and the CO_2-C_6H_6 mixture showed 9 kJ/kg increase.

CO_2-R152a and CO_2-C_6H_6 mixtures stand out as better options for use in supercritical cycles that recover waste heat. They offer higher efficiency and specific work over a wide range of compressor inlet temperatures, ranging from 40 °C to 65 °C, which corresponds to ambient temperatures of about 25 °C to 50 °C. This study highlights the significant potential of these mixtures for delivering higher thermodynamic performance in different temperature conditions. Future research will focus on exploring more mixtures and cycle layouts and assessing their economic feasibility.

CRediT authorship contribution statement

Al Bara Shalaby: Writing – original draft, Formal analysis, Data curation. **Nadeem Ahmed Sheikh:** Writing – review & editing, Supervision, Methodology, Investigation. **Abubakr Ayub:** Validation, Methodology, Formal analysis. **Muhammad Imran:** Writing – review & editing, Formal analysis. **Muhammad Wakil Shahzad:** Writing – review & editing, Conceptualization.

Declaration of competing interest

The authors declare that they have no known competing financial interests or personal relationships that could have appeared to influence the work reported in this paper.

Data availability

Data will be made available on request.

Appendix A

Simple recuperated cycle

Table A1
Experimental results of simple recuperated cycle.

F_{mol}		T_{min} (°C)	P_{exp} (MPa)	Thermal Efficiency		Cycle specific work (kJ/kg)	
R152a	C_6H_6			R152a	C_6H_6	R152a	C_6H_6
5	1	40	8	33.42	32.53	86.23	79.33
5	1	40	9	32.93	33.01	85.10	83.71
5	1	40	10	32.25	32.22	78.01	78.25
5	1	52.5	8	30.03	29.58	68.54	66.65
5	1	52.5	9	30.85	30.45	68.80	66.62
5	1	52.5	10	31.05	30.83	67.97	65.94
5	1	65	8	27.50	27.09	59.81	58.44
5	1	65	9	28.38	28.03	59.13	57.81
5	1	65	10	28.88	28.60	57.78	56.52
10	2.3	40	8	33.57	33.36	93.57	86.48
10	2.3	40	9	32.85	32.89	85.44	86.13
10	2.3	40	10	32.56	32.20	77.40	78.83
10	2.3	52.5	8	30.85	30.06	72.73	69.03
10	2.3	52.5	9	31.55	30.85	74.00	69.21
10	2.3	52.5	10	31.26	31.08	70.99	68.67
10	2.3	65	8	28.16	27.45	62.41	59.94
10	2.3	65	9	28.96	28.35	61.81	59.35
10	2.3	65	10	29.35	28.87	60.43	58.11
15	3.6	40	8	33.42	33.54	93.52	92.14
15	3.6	40	9	33.09	32.78	84.57	86.98
15	3.6	40	10	32.98	32.30	76.26	78.95
15	3.6	52.5	8	31.94	30.61	79.57	72.15
15	3.6	52.5	9	31.87	31.28	78.05	72.52
15	3.6	52.5	10	31.39	31.22	71.89	71.29
15	3.6	65	8	28.83	28.10	65.31	62.55
15	3.6	65	9	29.58	28.77	64.98	61.39
15	3.6	65	10	29.77	29.16	63.24	59.89

Recompression cycle

Table A2
Experimental results of recompression cycle.

F_{mol}		T_{min} (°C)	P_{exp} (MPa)	X_{split}	Thermal Efficiency		Cycle specific work (kJ/kg)	
R152a	C_6H_6				R152a	C_6H_6	R152a	C_6H_6
5	1	40	8	0.6	30.8	–	56.36	–
5	1	40	8	0.7	34.88	32.15	66.05	59.23
5	1	52.5	8	0.7	27.47	–	48.96	–
5	1	40	8	0.8	34.59	33.35	72.00	65.91
5	1	52.5	8	0.8	30.44	29.77	56.21	54.12
5	1	65	8	0.8	26.82	–	47.62	–
5	1	40	9	0.6	35.17	34.03	64.50	60.77

(*continued on next page*)

Table A2 (*continued*)

F_{mol}		T_{min} (°C)	P_{exp} (MPa)	X_{split}	Thermal Efficiency		Cycle specific work (kJ/kg)	
R152a	C_6H_6				R152a	C_6H_6	R152a	C_6H_6
5	1	52.5	9	0.6	26.53	24.96	44.08	41.02
5	1	40	9	0.7	36.94	36.58	71.41	68.49
5	1	52.5	9	0.7	30.60	29.35	52.50	49.73
5	1	65	9	0.7	25.75	24.78	42.55	40.69
5	1	40	9	0.8	36.46	35.38	76.07	73.12
5	1	52.5	9	0.8	31.92	31.29	58.05	55.70
5	1	65	9	0.8	28.85	28.08	48.75	47.13
5	1	40	10	0.6	35.00	34.98	61.61	60.87
5	1	52.5	10	0.6	29.87	28.41	48.13	44.98
5	1	65	10	0.6	24.11	22.98	36.92	34.89
5	1	40	10	0.7	36.59	36.48	67.29	66.68
5	1	52.5	10	0.7	32.87	31.80	54.73	51.96
5	1	65	10	0.7	27.86	26.99	43.88	42.14
5	1	40	10	0.8	36.49	36.46	71.14	70.77
5	1	52.5	10	0.8	32.73	32.25	58.92	56.53
5	1	65	10	0.8	29.86	29.40	48.81	47.35
10	2.3	40	8	0.6	35.78	30.96	70.41	56.96
10	2.3	40	8	0.7	37.54	35.05	78.20	66.85
10	2.3	52.5	8	0.7	29.68	27.52	53.96	49.27
10	2.3	40	8	0.8	36.92	34.61	83.49	72.67
10	2.3	52.5	8	0.8	31.62	30.47	60.53	56.60
10	2.3	65	8	0.8	28.20	–	50.67	–
10	2.3	40	9	0.6	35.52	35.43	67.00	65.54
10	2.3	52.5	9	0.6	29.67	26.47	50.90	44.16
10	2.3	65	9	0.6	23.20	–	37.82	–
10	2.3	40	9	0.7	37.14	36.92	73.46	72.36
10	2.3	52.5	9	0.7	33.07	30.58	58.72	52.62
10	2.3	65	9	0.7	27.37	25.66	45.92	42.54
10	2.3	40	9	0.8	36.76	36.71	77.74	77.21
10	2.3	52.5	9	0.8	33.09	31.88	63.59	58.28
10	2.3	65	9	0.8	29.75	28.78	51.68	48.83
10	2.3	40	10	0.6	34.75	35.16	62.36	62.39
10	2.3	52.5	10	0.6	31.81	29.96	53.14	48.48
10	2.3	65	10	0.6	26.02	24.03	40.62	36.91
10	2.3	40	10	0.7	36.28	36.55	67.73	68.04
10	2.3	52.5	10	0.7	34.23	33.01	59.22	55.21
10	2.3	65	10	0.7	29.35	27.83	47.19	43.97
10	2.3	40	10	0.8	36.19	36.63	71.23	71.98
10	2.3	52.5	10	0.8	33.38	32.74	62.90	59.47
10	2.3	65	10	0.8	30.65	29.83	51.74	49.01
15	3.6	40	8	0.6	36.02	33.72	72.63	64.29
15	3.6	52.5	8	0.6	28.81	–	52.31	–
15	3.6	40	8	0.7	37.67	36.72	79.99	73.31
15	3.6	52.5	8	0.7	32.71	29.10	61.50	52.92
15	3.6	65	8	0.7	26.43	–	47.08	–
15	3.6	40	8	0.8	37.03	35.23	84.77	78.54
15	3.6	52.5	8	0.8	33.18	31.28	67.28	59.84
15	3.6	65	8	0.8	29.34	28.00	53.85	50.51
15	3.6	40	9	0.6	35.23	35.80	67.48	67.72
15	3.6	52.5	9	0.6	32.28	28.18	57.77	47.88
15	3.6	65	9	0.6	25.36	22.36	42.12	36.46
15	3.6	40	9	0.7	36.91	37.05	73.75	74.25
15	3.6	52.5	9	0.7	34.93	31.94	64.80	56.07
15	3.6	65	9	0.7	29.08	26.79	49.77	44.95
15	3.6	40	9	0.8	36.38	–	77.60	–
15	3.6	52.5	9	0.8	33.96	32.49	69.00	61.37
15	3.6	65	9	0.8	30.69	29.42	55.08	51.00
15	3.6	40	10	0.6	34.26	35.11	62.30	63.32
15	3.6	52.5	10	0.6	32.48	31.45	55.75	52.25
15	3.6	65	10	0.6	27.91	25.18	44.64	39.21
15	3.6	40	10	0.7	35.60	36.44	67.33	68.79
15	3.6	52.5	10	0.7	34.47	34.11	61.37	58.67
15	3.6	65	10	0.7	30.80	28.72	50.82	46.01
15	3.6	40	10	0.8	35.63	36.53	70.65	72.57
15	3.6	52.5	10	0.8	33.81	33.16	64.86	62.59
15	3.6	65	10	0.8	31.42	30.28	55.00	50.86

Appendix B

Regression equations

Table B1
Regression equations for efficiency and cycle specific work of both cycles.

Cycle	Additive	Response	Equation
Simple cycle	R152a	Efficiency	39.36 + 0.105 *Fmol* − 0.3788 *Tmin* + 1.09 *Pexp* − 0.00021 *Fmol*Fmol* − 0.001811 *Tmin*Tmin* − 0.163 *Pexp*Pexp* + 0.00337 *Fmol*Tmin* − 0.0215 *Fmol*Pexp* + 0.04088 *Tmin*Pexp*
	R152a	Cycle specific work	167.5 + 2.51 Fmol − 3.574 Tmin + 5.1 Pexp − 0.0197 Fmol*Fmol + 0.00352 Tmin*Tmin − 1.006 Pexp*Pexp + 0.01571 Fmol*Tmin − 0.270 Fmol*Pexp + 0.2372 Tmin*Pexp
	C_6H_6	Efficiency	36.11 + 1.025 Fmol − 0.4982 Tmin + 2.23 Pexp − 0.0045 Fmol*Fmol − 0.000956 Tmin*Tmin − 0.2245 Pexp*Pexp + 0.00753 Fmol*Tmin − 0.1298 Fmol*Pexp + 0.04463 Tmin*Pexp
	C_6H_6	Cycle specific work	90.0 + 11.01 Fmol − 3.346 Tmin + 19.1 Pexp − 0.013 Fmol*Fmol + 0.01446 Tmin*Tmin − 1.349 Pexp*Pexp − 0.0294 Fmol*Tmin − 0.834 Fmol*Pexp + 0.1035 Tmin*Pexp
Recompression	R152a	Efficiency	− 49.5 + 1.993 Fmol − 1.905 Tmin + 12.03 Pexp + 182.5 Xsplit − 0.01388 Fmol*Fmol − 0.00129 Tmin*Tmin − 0.547 Pexp*Pexp − 106.7 Xsplit*Xsplit + 0.01066 Fmol*Tmin − 0.1421 Fmol*Pexp − 1.055 Fmol*Xsplit + 0.0943 Tmin*Pexp + 1.013 Tmin*Xsplit − 6.25 Pexp*Xsplit
	R152a	Cycle specific work	− 100.3 + 5.60 Fmol − 4.800 Tmin + 31.76 Pexp + 324.7 Xsplit − 0.0369 Fmol*Fmol + 0.00585 Tmin*Tmin − 1.664 Pexp*Pexp − 106.0 Xsplit*Xsplit + 0.01393 Fmol*Tmin − 0.4097 Fmol*Pexp − 1.538 Fmol*Xsplit + 0.2620 Tmin*Pexp + 0.874 Tmin*Xsplit − 15.76 Pexp*Xsplit
	C_6H_6	Efficiency	− 80.7 + 5.97 Fmol − 2.090 Tmin + 18.22 Pexp + 198.2 Xsplit − 0.0289 Fmol*Fmol + 0.00191 Tmin*Tmin − 0.715 Pexp*Pexp − 112.6 Xsplit*Xsplit + 0.01641 Fmol*Tmin − 0.425 Fmol*Pexp − 2.891 Fmol*Xsplit + 0.0651 Tmin*Pexp + 1.202 Tmin*Xsplit − 8.04 Pexp*Xsplit
	C_6H_6	Cycle specific work	− 229.6 + 16.46 Fmol − 4.595 Tmin + 56.00 Pexp + 349.4 Xsplit − 0.058 Fmol*Fmol + 0.01566 Tmin*Tmin − 2.536 Pexp*Pexp − 116.5 Xsplit*Xsplit − 0.0075 Fmol*Tmin − 1.248 Fmol*Pexp − 2.73 Fmol*Xsplit + 0.1390 Tmin*Pexp + 0.853 Tmin*Xsplit − 17.11 Pexp*Xsplit

Appendix C

Multi-objective optimization results

Table C1
Multi-Objective optimization results of R152a additive in recompression cycle.

Sr	Efficiency	Specific work	F_{mol}	T_{min}	P_{exp}	X_{split}
1	37.66	81.23	15.00	40.00	8.09	0.75
2	37.25	83.87	14.99	40.00	8.00	0.80
3	37.57	82.33	14.99	40.00	8.01	0.76
4	37.64	81.66	15.00	40.00	8.04	0.75
5	37.70	80.08	15.00	40.00	8.24	0.73
6	37.70	80.44	15.00	40.00	8.22	0.74
7	37.53	82.62	14.99	40.00	8.03	0.77
8	37.58	82.25	15.00	40.01	8.02	0.76
9	37.47	82.99	14.99	40.00	8.00	0.78
10	37.71	79.96	15.00	40.00	8.25	0.73
11	37.56	82.43	15.00	40.00	8.01	0.77
12	37.59	82.17	15.00	40.00	8.01	0.76
13	37.36	83.47	14.99	40.00	8.01	0.79
14	37.69	80.73	15.00	40.00	8.21	0.74
15	37.62	81.80	14.99	40.00	8.05	0.76
16	37.55	82.54	15.00	40.00	8.01	0.77
17	37.60	82.05	15.00	40.00	8.06	0.76
18	37.67	81.14	15.00	40.00	8.11	0.75
19	37.30	83.65	15.00	40.00	8.02	0.79
20	37.66	81.33	15.00	40.00	8.09	0.75
21	37.69	80.61	15.00	40.00	8.19	0.74
22	37.27	83.79	15.00	40.00	8.01	0.80
23	37.45	83.06	15.00	40.00	8.01	0.78
24	37.34	83.55	15.00	40.00	8.01	0.79
25	37.23	83.93	15.00	40.00	8.00	0.80
26	37.70	80.28	15.00	40.00	8.25	0.74
27	37.63	81.74	14.99	40.00	8.05	0.75
28	37.55	82.47	15.00	40.00	8.02	0.77
29	37.54	82.59	15.00	40.00	8.01	0.77
30	37.33	83.56	15.00	40.00	8.01	0.79
31	37.40	83.31	14.99	40.00	8.01	0.79
32	37.48	82.90	14.99	40.00	8.01	0.78
33	37.30	83.60	15.00	40.00	8.03	0.79
34	37.68	80.82	15.00	40.00	8.15	0.74
35	37.70	80.16	15.00	40.00	8.24	0.73
36	37.28	83.72	15.00	40.00	8.02	0.80
37	37.40	83.29	14.99	40.00	8.01	0.79
38	37.42	83.20	15.00	40.00	8.01	0.78
39	37.69	80.53	15.00	40.00	8.22	0.74
40	37.50	82.78	15.00	40.01	8.01	0.77

Table C2
Multi-Objective optimization results of C6H6 additive in recompression cycle.

Sr	Efficiency	Specific work	F_{mol}	T_{min}	P_{exp}	X_{split}
1	36.68	78.81	3.60	40.01	8.75	0.80
2	37.15	77.15	3.60	40.01	9.00	0.77
3	37.40	75.34	3.59	40.01	9.24	0.73
4	37.20	76.89	3.60	40.01	9.03	0.76
5	37.46	74.17	3.59	40.00	9.46	0.72
6	37.01	77.78	3.60	40.01	8.86	0.78
7	37.22	76.77	3.59	40.01	9.06	0.76
8	36.77	78.57	3.60	40.01	8.76	0.79
9	37.43	74.89	3.59	40.00	9.31	0.73
10	37.44	74.69	3.59	40.00	9.34	0.73
11	36.80	78.48	3.60	40.01	8.80	0.79
12	37.18	76.98	3.59	40.01	9.01	0.76
13	37.08	77.47	3.59	40.01	8.93	0.77
14	37.32	76.09	3.59	40.01	9.11	0.75
15	37.30	76.23	3.59	40.01	9.12	0.75
16	37.34	75.94	3.59	40.01	9.18	0.75
17	36.82	78.41	3.59	40.01	8.82	0.79
18	36.72	78.65	3.60	40.01	8.87	0.80
19	37.45	74.44	3.59	40.00	9.35	0.72
20	37.05	77.58	3.59	40.01	8.88	0.77
21	36.88	78.21	3.60	40.01	8.80	0.78
22	37.02	77.71	3.60	40.01	8.94	0.78
23	37.36	75.78	3.60	40.01	9.15	0.74
24	37.41	75.22	3.59	40.01	9.25	0.73
25	37.26	76.54	3.59	40.01	9.11	0.76
26	37.29	76.28	3.59	40.01	9.15	0.75
27	36.99	77.87	3.60	40.01	8.87	0.78
28	37.45	74.28	3.60	40.02	9.36	0.72
29	37.44	74.74	3.59	40.00	9.32	0.73
30	37.45	74.49	3.59	40.02	9.33	0.72
31	37.27	76.48	3.59	40.01	9.08	0.75
32	36.87	78.26	3.60	40.01	8.80	0.79
33	36.93	78.06	3.60	40.01	8.86	0.78
34	37.37	75.61	3.60	40.01	9.18	0.74
35	37.24	76.66	3.59	40.00	9.09	0.76
36	37.09	77.33	3.59	40.01	8.86	0.77
37	37.13	77.25	3.60	40.01	8.97	0.77
38	37.17	77.06	3.59	40.01	8.96	0.76
39	37.41	75.09	3.59	40.01	9.33	0.73
40	36.68	78.81	3.60	40.01	8.75	0.80

References

[1] A.G. Olabi, et al., Application of nanofluids for enhanced waste heat recovery: a review, Nano Energy 84 (Jun. 2021) 105871, https://doi.org/10.1016/J.NANOEN.2021.105871.

[2] S. Brueckner, L. Miró, L.F. Cabeza, M. Pehnt, E. Laevemann, Methods to estimate the industrial waste heat potential of regions – a categorization and literature review, Renew. Sust. Energ. Rev. 38 (Oct. 2014) 164–171, https://doi.org/10.1016/J.RSER.2014.04.078.

[3] C. Forman, I.K. Muritala, R. Pardemann, B. Meyer, Estimating the global waste heat potential, Renew. Sust. Energ. Rev. 57 (May 2016) 1568–1579, https://doi.org/10.1016/J.RSER.2015.12.192.

[4] N. Galanis, E. Cayer, P. Roy, E.S. Denis, M. Désilets, Electricity generation from low temperature sources, J. Appl. Fluid Mechan. 2 (2) (Jan. 2012) 55–67, https://doi.org/10.36884/JAFM.2.02.11870.

[5] M. Papapetrou, G. Kosmadakis, A. Cipollina, U. la Commare, G. Micale, Industrial waste heat: estimation of the technically available resource in the EU per industrial sector, temperature level and country, Appl. Therm. Eng. 138 (Jun. 2018) 207–216, https://doi.org/10.1016/J.APPLTHERMALENG.2018.04.043.

[6] D. Vance, et al., Estimation of and barriers to waste heat recovery from harsh environments in industrial processes, J. Clean. Prod. 222 (Jun. 2019) 539–549, https://doi.org/10.1016/J.JCLEPRO.2019.03.011.

[7] A. Firth, B. Zhang, A. Yang, Quantification of global waste heat and its environmental effects, Appl. Energy 235 (Feb. 2019) 1314–1334, https://doi.org/10.1016/J.APENERGY.2018.10.102.

[8] L. Liu, Q. Yang, G. Cui, Supercritical carbon dioxide(s-CO2) power cycle for waste heat recovery: a review from thermodynamic perspective, Processes 8 (11) (Nov. 2020) 1461, https://doi.org/10.3390/PR8111461.

[9] Epa and CHP, Waste Heat to Power Systems [Online]. Available, https://www.energy.gov/sites/default/files/2016/04/f30/CHP%20Technical%20Potential%20Study%203-31-, 2024.

[10] E. Macchi, M. Astolfi, Organic Rankine Cycle (ORC) Power Systems: Technologies and Applications, Woodhead Publishing, 2016.

[11] C.M. Invernizzi, D. Bonalumi, Thermal stability of organic fluids for Organic Rankine Cycle systems, in: Organic Rankine Cycle (ORC) Power Systems: Technologies and Applications, Jan. 2017, pp. 121–151, https://doi.org/10.1016/B978-0-08-100510-1.00005-3.

[12] E.G. Feher, The supercritical thermodynamic power cycle, Energy Convers. 8 (2) (Sep. 1968) 85–90, https://doi.org/10.1016/0013-7480(68)90105-8.

[13] C. Li, H. Wang, Power cycles for waste heat recovery from medium to high temperature flue gas sources – from a view of thermodynamic optimization, Appl. Energy 180 (Oct. 2016) 707–721, https://doi.org/10.1016/J.APENERGY.2016.08.007.

[14] Vaclav Dostal, J.A. Coderre, A Supercritical Carbon Dioxide Cycle for Next Generation Nuclear Reactors Certified by A Chairman, Department Committee on Graduate Students, Dipl. Ing., Mechanical Engineering, 2000.

[15] S.J. Bae, J. Lee, Y. Ahn, J.I. Lee, Preliminary studies of compact Brayton cycle performance for small modular high temperature gas-cooled reactor system, Ann. Nucl. Energy 75 (Jan. 2015) 11–19, https://doi.org/10.1016/J.ANUCENE.2014.07.041.

[16] S.-P. Kao, CANES Center for Advanced Nuclear Energy Systems Application of Supercritical CO 2 Brayton Cycle for Small Modular Light Water Reactors 2016 International Congress on Advances in Nuclear Power Plants, 2024.

[17] T. Neises, C. Turchi, A comparison of supercritical carbon dioxide power cycle configurations with an emphasis on CSP applications, Energy Procedia 49 (Jan. 2014) 1187–1196, https://doi.org/10.1016/J.EGYPRO.2014.03.128.

[18] P. Huck, S. Freund, M. Lehar, M. Peter, The 5 th International Symposium-Supercritical CO2 Power Cycles Performance Comparison of Supercritical CO 2 versus Steam Bottoming Cycles for Gas Turbine Combined Cycle Applications, 2024.

[19] M. Astolfi, D. Alfani, S. Lasala, E. Macchi, Comparison between ORC and CO2 power systems for the exploitation of low-medium temperature heat sources, Energy 161 (Oct. 2018) 1250–1261, https://doi.org/10.1016/J.ENERGY.2018.07.099.

[20] Xie, (2) United States Patent (54) (71) (72) (73) (*) (21) (22) (65) (60) (51) (52) (58), 2016.

[21] M. Mohagheghi, J. Kapat, Thermodynamic optimization of recuperated S-CO2 Brayton cycles for waste heat recovery applications, in: 4th International Supercritical CO2 Power Cycles Symposium, 2014.
[22] G.S. Martínez, D. Sánchez, F. Crespi, G. Gavagnin, A global approach to assessing the potential of combined cycles using supercritical technology, in: Proceedings of the 1st Global Power and Propulsion Forum (GPPF), Zurich, Switzerland, 2017, pp. 16–18.
[23] G. Manente, M. Costa, On the conceptual design of novel supercritical CO2 power cycles for waste heat recovery, Energies (Basel) 13 (2) (2020), https://doi.org/10.3390/en13020370.
[24] J. Song, X. Li, X. Ren, C. Gu, Performance improvement of a preheating supercritical CO2 (S-CO2) cycle based system for engine waste heat recovery, Energy Convers. Manag. 161 (2018) 225–233.
[25] M. Ahmed, A. Ayub, N.A. Sheikh, M.W. Shahzad, M. Haroon, M. Imran, Thermodynamic optimization and performance study of supercritical CO2 thermodynamic power cycles with dry cooling using response surface method, Int. Commun. Heat Mass Transf. 142 (Mar. 2023), https://doi.org/10.1016/j.icheatmasstransfer.2023.106675.
[26] D. Bonalumi, S. Lasala, E. Macchi, CO2-TiCl4 working fluid for high-temperature heat source power cycles and solar application, Renew. Energy 147 (Mar. 2020) 2842–2854, https://doi.org/10.1016/J.RENENE.2018.10.018.
[27] E. Morosini, G. Manzolini, G. di Marcoberardino, C. Invernizzi, P. Iora, Investigation of CO2 mixtures to overcome the limits of sCO2 cycles, in: 76th Italian National Congress ATI 2021, ATI, 2021, pp. 8010–8019.
[28] G. di Marcoberardino, et al., Experimental and analytical procedure for the characterization of innovative working fluids for power plants applications, Appl. Therm. Eng. 178 (Sep. 2020) 115513, https://doi.org/10.1016/J.APPLTHERMALENG.2020.115513.
[29] G. Di Marcoberardino, et al., Experimental characterisation of CO2+ C6F6 mixture: thermal stability and vapour liquid equilibrium test for its application in transcritical power cycle, Appl. Therm. Eng. 212 (2022) 118520.
[30] P. Tafur-Escanta, R. Valencia-Chapi, I. López-Paniagua, L. Coco-Enríquez, J. Muñoz-Antón, Supercritical CO2 Binary Mixtures for Recompression Brayton S-CO2 Power Cycles Coupled to Solar Thermal Energy Plants, 2021.
[31] Y.-N. Ma, P. Hu, C.-Q. Jia, Z.-R. Wu, Q. Chen, Thermo-economic analysis and multi-objective optimization of supercritical Brayton cycles with CO2-based mixtures, Appl. Therm. Eng. 219 (2023) 119492.
[32] Y. Yang, T. Xue, Z. Rao, S. Liao, Potential of transcritical recompression Rankine cycle operating with CO2-based binary mixtures, Energy Convers. Manag. 252 (2022) 115040.
[33] Y. Ma, M. Liu, J. Yan, J. Liu, Performance investigation of a novel closed Brayton cycle using supercritical CO2-based mixture as working fluid integrated with a LiBr absorption chiller, Appl. Therm. Eng. 141 (2018) 531–547.
[34] X. Liu, Z. Xu, Y. Xie, H. Yang, CO2-based mixture working fluids used for the dry-cooling supercritical Brayton cycle: thermodynamic evaluation, Appl. Therm. Eng. 162 (2019) 114226.
[35] Gas Servei, Accessed: Jun. 17, 2023. [Online]. Available: https://gas-servei.com/en/biblioteca/#documentacion, 2024.
[36] Praxair, Accessed: Jun. 17, 2023. [Online]. Available: www.praxair.com, 2024.
[37] Cameo, Accessed: Jun. 01, 2023. [Online]. Available: https://cameochemicals.noaa.gov/chris/BNZ.pdf, 2024.
[38] Aspen Plus, Accessed: Jun. 17, 2023. [Online]. Available: https://www.aspentech.com/en/products/engineering/aspen-plus, 2024.
[39] NFPA, Accessed: Jun. 17, 2023. [Online]. Available: https://www.nfpa.org/Codes-and-Standards, 2024.
[40] A. Ayub, G. Marcoberardini, C. Invernizzi, P. Iora, Advanced thermodynamic power cycles utilizing carbon dioxide based mixtures as working fluids for high temperature waste heat recovery, in: 4th European sCO2 Conference for Energy Systems: March 23–24, 2021, Online Conference, Mar. 2021, pp. 58–67, https://doi.org/10.17185/duepublico/73947.
[41] G. Di Marcoberardino, et al., Experimental and analytical procedure for the characterization of innovative working fluids for power plants applications, Appl. Therm. Eng. 178 (May) (Sep. 2020) 115513, https://doi.org/10.1016/j.applthermaleng.2020.115513.
[42] J.W. Kang, A.R. Kim, J.S. Lim, High pressure isothermal vapor-liquid equilibria of carbon dioxide+1,1-difluoroethane, Korean J. Chem. Eng. 27 (1) (Feb. 2010) 261–266, https://doi.org/10.1007/S11814-009-0334-0.
[43] H. Madani, A. Valtz, C. Coquelet, A.H. Meniai, D. Richon, (Vapor + liquid) equilibrium data for (carbon dioxide + 1,1-difluoroethane) system at temperatures from (258 to 343) K and pressures up to about 8 MPa, J. Chem. Thermodyn. 40 (10) (Oct. 2008) 1490–1494, https://doi.org/10.1016/J.JCT.2008.06.002.
[44] K. Ohgaki, T. Katayama, Isothermal vapor-liquid equilibrium data for binary systems containing carbon dioxide at high pressures: methanol–carbon dioxide, n-Hexane–Carbon Dioxide, and Benzene–Carbon Dioxide Systems, J. Chem. Eng. Data 21 (1) (Jan. 1976) 53–55, https://doi.org/10.1021/JE60068A015/ASSET/JE60068A015.FP.PNG_V03.
[45] C.H. Kim, P. Vimalchand, M.D. Donohue, Vapor-liquid equilibria for binary mixtures of carbon dioxide with benzene, toluene and p-xylene, Fluid Phase Equilib. 31 (3) (Jan. 1986) 299–311, https://doi.org/10.1016/0378-3812(86)87014-5.
[46] Critical lines and phase equilibria in binary van der Waals mixtures, Philosoph. Trans. Royal Soc. Lond. Ser. A Math. Phys. Sci. 298 (1442) (Dec. 1980) 495–540, https://doi.org/10.1098/RSTA.1980.0266.
[47] G. Manente, F.M. Fortuna, Supercritical CO2 power cycles for waste heat recovery: a systematic comparison between traditional and novel layouts with dual expansion, Energy Convers. Manag. 197 (July) (Oct. 2019) 111777, https://doi.org/10.1016/j.enconman.2019.111777.
[48] M. Marchionni, G. Bianchi, S.A. Tassou, Review of supercritical carbon dioxide (sCO2) technologies for high-grade waste heat to power conversion, SN Appl. Sci. 2 (4) (Apr. 2020) 611, https://doi.org/10.1007/s42452-020-2116-6.
[49] G. Angelino, Carbon dioxide condensation cycles for power production, J. Eng. Power 90 (3) (Jul. 1968) 287–295, https://doi.org/10.1115/1.3609190.
[50] E. Morosini, A. Ayub, G. di Marcoberardino, C.M. Invernizzi, P. Iora, G. Manzolini, Adoption of the CO2 + SO2 mixture as working fluid for transcritical cycles: a thermodynamic assessment with optimized equation of state, Energy Convers. Manag. 255 (Mar. 2022) 115263, https://doi.org/10.1016/J.ENCONMAN.2022.115263.
[51] G. Manente, F.M. Fortuna, Supercritical CO2 power cycles for waste heat recovery: a systematic comparison between traditional and novel layouts with dual expansion, Energy Convers. Manag. 197 (2019) 111777.
[52] R. Valencia-Chapi, L. Coco-Enríquez, J. Muñoz-Antón, Comparing line-focusing and central tower solar power plants with s-CO2 binary mixture Brayton power cycles, in: AIP Conference Proceedings, AIP Publishing LLC, 2020, 130010.
[53] J. Xia, J. Wang, G. Zhang, J. Lou, P. Zhao, Y. Dai, Thermo-economic analysis and comparative study of transcritical power cycles using CO2-based mixtures as working fluids, Appl. Therm. Eng. 144 (Nov. 2018) 31–44, https://doi.org/10.1016/j.applthermaleng.2018.08.012.
[54] A.I. Khuri, S. Mukhopadhyay, Response surface methodology, Wiley Interdiscip. Rev. Comput. Stat. 2 (2) (Mar. 2010) 128–149, https://doi.org/10.1002/WICS.73.
[55] K.M. Carley, N.Y. Kamneva, J. Reminga, Response Surface Methodology 1 CASOS Technical Report, Accessed: Nov. 27, 2022. [Online]. Available: http://www.casos.cs.cmu, 2004.